UNIVERSITÀ DEGLI STUDI DI PADOVA

Dipartimento di Fisica e Astronomia
Corso di Laurea in Astronomia

Tesi di Laurea Magistrale

Dielectric models of Ganymede and Callisto's icy crust aimed to the estimate of the performance of RIME

Relatore:
Prof. Francesco Marzari
Correlatore:
Dr. Riccardo Claudi
Correlatore esterno:
Dr. Federico Di Paolo

Candidato:
Alessandro Ruggieri
Matricola: 1202390

Alessandro Ruggieri

Anno Accademico 2019-2020

Contents

Introduction

Radar sounding is a technique that has been expanding in the last years as a means to study the crusts of planetary bodies. In 2022 the ESA mission JUICE (JUpiter ICy moons Explorer) will be launched and, among the other instruments, it will carry the radar RIME (Radar for Icy Moon Exploration). This instrument is a 16 m antenna with a central frequency of 9 MHz ($\lambda = 18.62$ m in ice) and two possible bandwidths (1 and 3 MHz). In general terms, it will be used to probe the crust of Ganymede and Callisto, with an expected vertical resolution of a few tens of meters down to a few kilometers. This is possible because these bodies are mainly made up of water ice, which has a very low dielectric permittivity (around 3.2) in the radio part of the electromagnetic spectrum. On the other hand, this is not true for liquid water, whose dielectric permittivity has a value around 80. This means that, by analyzing the returned radar wave, it is possible to find an ice-water interface, if present. The consequence is that this technique allows the detection of a potential subsurface ocean, and other features, inside the icy satellites of the Solar System. The situation is more complicated since the ice of these bodies is not pure. Several chemical compounds, that have been not uniquely identified so far, locally change the dielectric permittivity of ice. This quantity is also affected by porosity and temperature, which change with depth.

The purpose of this work is to construct dielectric models for the crusts of Ganymede and Callisto, and to simulate the propagation of a radar wave having the same characteristics as those of RIME. Such models are based on reasonable assumptions about temperature profiles, porosity values, and abundances of chemical compounds taken from the literature. The most important parameter affecting these models is the presence of these impurities. For this reason, recent dielectric data taken from the literature will be used to simulate the possible internal compositions of Ganymede and Callisto. Most of the literature agrees that convection is unlikely to occur inside these two satellites, therefore the temperature profile will be assumed to purely conductive. The aim is to determine whether it is possible to detect specific features under the surface at a given depth. This is done by calculating the cumulative attenuation, which indicates how weak the returned radio signal is compared to the transmitted one. The greater is

the cumulative attenuation, the smaller will be the penetration depth, that is the maximum depth that we can expect to probe. What's more, through the comparison between the models and future data, it will be possible to constrain the actual chemical composition.
In Chapter 1, I will give a useful theoretical background about the two satellites under consideration, with their unresolved problems, about the JUICE mission that will help to resolve some of such problems, and about the dielectric properties of ice, which make the work of RIME possible. In Chapter 2, I will discuss the possible chemical compositions of these two bodies according to the literature, and the possibility that they might have experienced differentiation. In Chapter 3, I will show the physical parameters that are needed to construct dielectric models: thermal, porosity, and chemical impurities gradients. I will also explain how these quantities affect the dielectric permittivity. In Chapter 4, I will show the model used for the simulations, the range in which the variables have been assumed to vary, and the results obtained, keeping an eye on the observational perspective. In particular, I will show how to calculate the cumulative attenuation and will compare the resulting values for this quantity with the observational limit that, according to the literature, should be around 55 dB due to several noise sources. I will also show the subsequent penetration depths in the different scenarios considered. In Chapter 5, I will resume the conclusions of this work.

Chapter 1

Theoretical background

1.1 Ganymede and Callisto

1.1.1 Physical and orbital parameters

Ganymede and Callisto are two of the four Galilean satellites of Jupiter, discovered by Galileo in 1610. They are the largest and the third-largest satellite of the Solar System, respectively. Both are important targets for future exploration since they have unique features. For example, Callisto is one of the most cratered bodies in the Solar System and its surface is therefore very old. This is not true for Ganymede, where some activity has occurred. They also have a good astrobiological potential, even though not as much as Europa or Titan, due to the possible presence of a subsurface ocean (e.g., Pappalardo et al. (2004)) that will be discussed later in this work. Table 1.1 shows the most important parameters of these two bodies. Ganymede and Callisto are found in a 1:2:4 Laplace resonance with Europa, and this causes the three satellites to experience a stronger tidal activity than their eccentricities would normally allow. Whether this resonance has a primordial origin (Peale and Lee, 2002) or was later formed due to long-term gravitational interactions (Yoder and Peale, 1981) is still unknown. Furthermore, they are, as many other satellites, in 1:1 spin-orbit resonance. Their densities are similar to each other, and smaller compared to those of the other Galilean satellites, Io and Europa. The explanation is quite clear for Io: since it is the most volcanically active body of the Solar System, water and other volatile compounds have all evaporated over time, leaving only the rocky part. This is not true for Europa, so the amount of non-water contaminants could be decreasing with increasing distance from Jupiter. On the other hand, Callisto seems to have a higher surficial abundance of rocks than Ganymede. However, this could be a simple apparent effect given by the lack of differentiation of Callisto, as confirmed by its slightly lower density.

	Ganymede	Callisto
M (10^{23} kg)	1.482	1.076
R (km)	2634.1 ± 0.3	2408.4 ± 0.3
ρ (g/cm^3)	1.936	1.839
Albedo (visible)	0.45	0.2
a (Jovian radii)	15.0	26.4
C/MR^2	0.3105 ± 0.0028	0.359 ± 0.005

Table 1.1: Physical and orbital parameters of Ganymede and Callisto (Calvin et al., 1995; Showman and Malhotra, 1999; Ogihara and Ida, 2012).

1.1.2 Surfaces

The surfaces of these two bodies are very interesting. The albedo varies from one point to the other, but it is generally higher on Ganymede than on Callisto. This should demonstrate that the former has a higher abundance of water ice than the latter, at least on the surface. This may not be true in general, since, as said, the two bodies probably experienced different degrees of differentiation. The surface of Callisto is, on average, more cratered and therefore older. Ganymede's surface is divided into dark and bright terrains: the former are more cratered, so older, with a higher abundance of chemical impurities, and represent about one-third of the total surface. They are more abundant on the trailing hemisphere. The thermal inertia is also different, indicating a different composition (Pappalardo et al., 2004). Ganymede's surface is made up of both smooth and rough terrains, indicating that there was geological activity at some point in the past. In particular, the dark terrains may have originated from the sputtering given by Jupiter's magnetosphere. These areas are also believed to have a thicker regolith layer. Salts are also present and may be due to resurfacing (Ligier et al., 2019b). In the overall, water ice is the main constituent. On Ganymede, ice is mostly amor-

phous at high latitudes in the jovian-facing hemisphere and at low latitudes in the trailing one (Dalton et al., 2010). On the other hand, ice is mostly crystalline on Callisto (Dalton et al., 2010). However, after 1 mm depth the ice becomes crystalline on both bodies. The temperature of Ganymede's surface ranges from 90 K at night to 150 K at day (Pappalardo et al., 2004). The temperature of Callisto's surface goes from 80 to 165 K (Moore et al., 2004).

1.1.3 Interior

Several models have been proposed for the interiors of Ganymede and Callisto. They are based on gravitational data, theoretical considerations, and geomagnetical data. As shown in Table 1.1, these two satellites have rather different values of C/MR^2, which is the adimensional momentum of inertia. This quantity is defined for a planetary body with values of the momentum of inertia around its main axis of inertia called A, B, and C for which $A < B < C$. Since C is divided by MR^2, with M mass of the body and R its mean radius, the quantity is adimensional. For a perfectly spherical body with uniform density, this quantity is equal to 0.4, therefore the real value measures the deviation from such an ideal case. The greater is the deviation and the greater is the concentration of denser material towards the center. In other words, a smaller value of this quantity indicates the presence of differentiation and of a planetary nucleus that is denser than the above layers. Ganymede has a lower value than Callisto, and this implies that the former has experienced a greater differentiation than the latter (Monteux et al., 2018). The total internal layering is not the aim of this work since the crusts of these satellites are expected to be at least 90 km and up to several hundred km thick (Showman and Malhotra, 1999; Sohl et al., 2002; Lucchetti et al., 2020), and RIME is likely able to reach a depth of about 9 km (Bruzzone et al., 2013). The internal structure of these satellites is important for this work under the two following points of view. First, the fact that they have experienced differentiation or not affects the presence of non-water impurities in the layers right under the surface. Even if Ganymede has, in the overall, a greater amount of rocky components, they are mostly found in the mantle or the nucleus due to the differentiation process. On the contrary, Callisto did not differentiate (or only partially), so the non-water substances should be more homogeneously distributed in the whole body. This affects the dielectric properties of the upper layers. The second important aspect is that both may have a subsurface ocean. The presence of such an ocean has been used to justify the induced magnetic fields of these bodies, and Europa too (e.g., Pappalardo et al. (2004)). For this to be possible, the ocean must be salty. However, heat transfer is expected to occur via convection on Europa (e.g., Heggy et al. (2017)) but not on Ganymede and Callisto. What's more, Europa is much closer to Jupiter ($a = 9.4$ jovian

radii) and therefore experiences a stronger tidal heating. Finally, the higher density suggests a greater amount of non-water substances. Salts can lower the melting temperature of ice. These facts together should imply that Europa's ocean should be at a much smaller depth than those of Ganymede and Callisto. As said, the ice crust above the putative ocean should be at least 90 km thick, therefore our current knowledge suggests that the ocean is unlikely to be detected by RIME.

1.2 Unresolved problems

There are still some unresolved problems regarding the Galilean satellites. The exact chemical composition of the surface is still unknown, even if there have been several attempts to determine it through infrared spectra (Moore et al., 2004; Dalton, 2010; Dalton et al., 2010; Ligier et al., 2019a,b,c, 2020). Some Mg- and S-based compounds have been identified, but there are still spectral features that remain unmatched. A particular problem is the origin of the sulfur that is present, since it may come both from Io's eruptions or from the interior, or even a combination of the two. The internal composition is poorly constrained as well, but it should be a mixture of water ice and silicates. Different possible combinations will be considered for the models in Chapter 4. In the literature, the internal thermal profiles of both Ganymede and Callisto are usually assumed to be conductive (e.g., Vance et al. (2014); Sotin et al. (2020)). However, this cannot be taken for granted, since convection is likely to occur inside Europa, and could, therefore, be in action inside the other two satellites as well. As already mentioned, the presence of an ocean is deduced by the presence of the induced magnetic fields, but gravitational data do not allow to distinguish between liquid and solid water, so the doubt remains. The depth of such putative ocean is still unknown too, since different models result in rather different allowed depths. Another unsolved problem that has already been mentioned concerns the origin of the Laplace resonance. One last problem regards the weird radar properties of the icy Galilean satellites. These have a radar albedo ≥ 1, corresponding to the backscatter efficiency of a large perfectly conducting sphere (while it is about 0.1 for terrestrial bodies). Moreover, when circularly polarized waves are transmitted, more echo power is received in the same circular sense of polarization than in the opposite sense, leading to a circular polarization ratio $\mu_C = \sigma_{sc}/\sigma_{oc} > 1$, where σ are the radar cross-sections for same- (SC) and opposite-circular (OC) polarization configurations of the transmitter-receiver combination ($\mu_C \sim 0.1 - 0.4$ for terrestrial bodies) (Baron et al., 2003). The radar cross-section decreases with the water ice purity, that is going from Europa to Callisto. Such properties are expected to be due to multiple volume scattering phenomena with very long photon paths, such as the coherent backscatter effect (Black et al., 2001), but there is no model

that can perfectly explain all the observed data.

1.3 The JUICE mission

JUICE (JUpiter ICy moons Explorer) is an ESA's mission that will be launched in 2022. It will arrive in the jovian system in January 2030 (Grasset et al., 2013). It will study the planet Jupiter, its satellites (Ganymede in particular), and the interactions that take place in the Jovian environment. During the first part, the spacecraft will focus on Jupiter and will perform two flybys at Europa. The RIME instrument will be at work during the closest approach to Europa, when the probe will be closer than 1000 km above the surface. Afterward, the probe will perform several Callisto's flybys to study this body and to change orbit. In September 2032, it will be inserted in orbit around Ganymede. The initial altitude will be around 5000 km, then it will drop to 500 km and finally to 200 km. The overall resolution across the surface of Ganymede will be around 400 m/px, with a higher resolution of a few m/px for some selected targets (Grasset et al., 2013). The nominal mission ends in June 2033, but it may be possible to extend it. One option is to keep the 200 km orbit to continue with plasma and magnetic field measurements. Alternatively, the probe can be let spiral down towards Ganymede to continue with observations of the surface.
RIME, as said, will have a central frequency of 9 MHz with two possible bandwidths (1 and 3 MHz), allowing a good penetration and a vertical resolution of a few tens of meters. This can be found be inserting the bandwidth value BW in the formula

$$\delta_r = \frac{c}{2BW n_{ice}} \tag{1.1}$$

which expresses the vertical resolution δ_r, with c speed of light, and n_{ice} the refractive index of ice Blankenship et al. (2009). The mission will also improve by three orders of magnitude the accuracy of the second-order gravitational coefficients measurements (Grasset et al., 2013), further constraining the internal layering of these satellites. JUICE will also measure the tidal response of the Galilean satellites and this, together with ground-based astrometric observations, will allow a better estimate of tidal energy dissipation. The high-resolution observations of the surface will allow a better constrain of the chemical composition.

1.4 Dielectric properties of water ice

As already said, RIME will be able to obtain useful data thanks to the peculiar properties of water ice. Since H_2O is a polar molecule, it has a permanent non-zero dipole moment. Normally, such momenta are randomly

distributed, so that the total polarization is zero. When an external field is applied, they orienteer themselves accordingly and the means is said to be polarized. This polarization is given by the sum of four contributions: electronic, atomic, dipolar, and ionic. Since these are given by mechanisms acting on different timescales, the total polarization depends on the frequency at which the external field changes. In particular, electronic polarization is the fastest one, while the ionic polarization is the slowest. In the end, the electric displacement field is given by

$$\overline{D} = \varepsilon_0 \overline{E} + \overline{P}, \tag{1.2}$$

which, for a homogeneous and isotropic means, becomes

$$\overline{D} = \varepsilon_0 (1 + \chi) \overline{E} = \varepsilon_0 \varepsilon_s \overline{E} \tag{1.3}$$

with P polarization density, ε_0 vacuum permittivity, ε_s static dielectric permittivity of the medium (that is the value assumed at low frequencies), $\overline{E}$ external electric field, and χ electric susceptibility. As a consequence, the dielectric permittivity decreases with increasing frequency, since if the electric field varies faster, not all the mentioned polarization processes can keep up with such variations. In particular, when the frequency of the electric field becomes greater than that typical of one of the four polarization mechanisms, the permittivity tends to the value ε_∞ relative to that frequency range. For example, water at room temperature has a real permittivity around 80 in the radio part of the spectrum, then it drops to around 5.6 in the IR domain and tends to 1 going towards the UV region. The limit of $\varepsilon = 1$ is the same for all materials at high frequencies, since at some point the electric field changes too fast even for electronic polarization. In the Debye model, the electric displacement vector is calculated considering the time delay given by the different timescales of the polarization mechanisms. In particular, this quantity depends on time and on a weight function that accounts for the values assumed by the electric field in the time range from zero to the time t considered. This weight function is assumed to be

$$f(t) = f(0) e^{-t/\tau} \tag{1.4}$$

with τ relaxation time that depends on the material and the temperature. In this way, it is possible to define the relative complex dielectric permittivity, whose real and imaginary part are

$$\varepsilon_r'(\omega) = \varepsilon_\infty + \frac{\varepsilon_s - \varepsilon_\infty}{1 + \omega^2 \tau^2} \text{ and } \varepsilon_r''(\omega) = \frac{(\varepsilon_s - \varepsilon_\infty)\omega\tau}{1 + \omega^2 \tau^2} \tag{1.5}$$

respectively, with ω frequency of the electric sinusoidal field. The total permittivity is given by $\varepsilon_r(\omega) = \varepsilon_r'(\omega) - i\varepsilon_r''(\omega)$. It is therefore possible to define the loss tangent as

$$\tan\left(\delta(\omega)\right) = \frac{\varepsilon_r''(\omega)}{\varepsilon_r'(\omega)}, \tag{1.6}$$

so the ratio between the real and the imaginary permittivity. The real part represents the energy stored in the dielectric medium, while the imaginary part represents the energy losses due to dissipation. Figure 1.1 shows how ε' and ε'' depend on frequency.

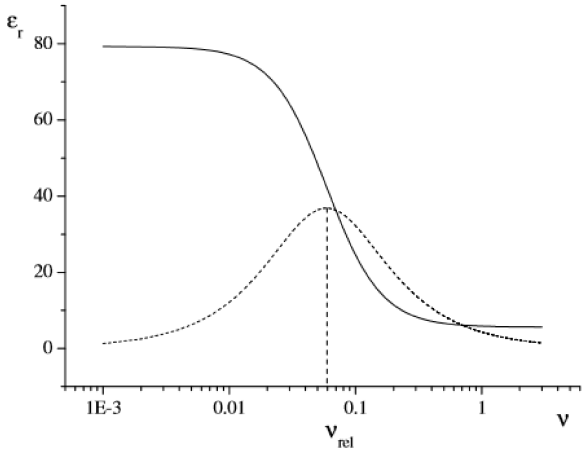

Figure 1.1: Real (continuous line) and imaginary (dashed line) dielectric permittivity as functions of the frequency, expressed in arbitrary units.

As shown, the imaginary part has a minimum in the same point in which the real part has an inflection point. This represents the relaxation frequency, given by $\nu_{rel} = (2\pi\tau)^{-1}$.
That being said, it is now interesting to report some facts about ice. In the 1 MHz - 10 GHz range, the real permittivity of pure water ice does not depend on frequency and ranges from 3.1 to 3.2 (slightly temperature dependent), while the imaginary part is lower than 10^{-3} (Brouet et al., 2016). Given the power transmitted by the radar, the power lost at a depth z through ice is given by

$$P(z)/P(0) = \exp\left[\frac{-4\pi z\varepsilon''}{\lambda\varepsilon'}\right], \tag{1.7}$$

with λ wavelength of the electromagnetic wave (Pappalardo et al., 1999). If the loss tangent is $\tan(\delta) \ll 1$, as it is the case for water ice, the attenuation can be expressed as

$$A_{\mathrm{dB/km}} \approx 0.091\sqrt{\varepsilon'}\nu\tan(\delta)\ \mathrm{dB/m} \tag{1.8}$$

with ν frequency expressed in MHz (Chyba et al., 1998). For water ice, the resulting attenuation has typical values between 4 and 10 dB/km (Kofman and Safaeinili, 2004). However, this does not take into account the presence of non-water contaminants, which increase attenuation. This quantity increases at higher temperatures. In particular, if convection is going on inside these bodies, this will greatly enhance attenuation (McKinnon, 2005) due to the higher temperature implied. In such an unlikely case, the radar will be able to reach depths similar to the conductive case only in the cold downwellings.

Chapter 2

Chemical composition

2.1 Differentiation

The possibility that Ganymede and Callisto may have experienced differentiation has already been mentioned in the previous chapter. As said, they both have a magnetic field induced by the strong Jovian field. This is the main argument in favor of the presence of a subsurface salty ocean (Showman and Malhotra, 1999), since the presence of a liquid layer cannot be retrieved by gravitational data alone. In the past, this ocean must have been closer to the surface than it is today, since planetary bodies are rather hot when they form (due to accretion and, possibly, differentiation) and then cool down as time passes. In particular, these satellites have approximately the same size as Mercury but lie much further away from the Sun, therefore they must have lost a great part of their primordial heat. The natural consequence is that the ocean should be very deep, as already said. However, it should be closer to the surface on Ganymede than on Callisto, for three reasons. First, because Ganymede has experienced a greater degree of differentiation, as demonstrated by the lower C/MR^2. Differentiation is an important source of energy in planetary bodies, and can help to maintain a liquid layer. Secondly, the amount of non-water substances is likely to decrease with increasing distance from Jupiter. This is similar, although on a smaller scale, to what happens for the metal content of planets at increasing distance from the Sun. In any case, such an effect should be demonstrated by the fact that Europa has a higher density than Ganymede, which has a higher density than Callisto. These non-water contaminants can contribute to the total heat of these bodies via radiogenic decay. In particular, it has been estimated that the radiogenic heat inside Callisto is 70% of that of Ganymede (Kimura and Kuramoto, 2010). What's more, Ganymede is closer to Jupiter, so tidal activity, if present, should be slightly stronger. Finally, the presence of substances such as salts or ammonia can allow the ocean to be closer to the surface than it otherwise could.

Another important aspect is that Ganymede has an intrinsic magnetic field. This is remarkable, since it is the only satellite known to display such a particular feature. Planetary magnetic fields are believed to be originated via dynamo effect. A body requires a partially liquid and metallic core with free electrons. If these charges can move fast enough, they give rise to an electric current that generates a magnetic field. The required motion is impressed by the rotation of the planet. This model explains the magnetic fields of the inner planets. In the case of Ganymede, the presence of the intrinsic field should imply that the core is metallic and at least partially melt. Callisto does not have an intrinsic field, therefore he must lack one of the two mentioned requirements. It could be that its $\sim$ 16-days rotation period is too long, since it is more than twice that of Ganymede. The total mass and density are rather close to the Ganymedian values, so the initial heat and the amount of rocky material cannot be too different. The lack of differentiation could explain this difference, implying that not all the metallic and rocky components have sunk towards the center, and therefore Callisto has not developed a large, dense, and partially melt nucleus like Ganymede. The point here is to underline that, even though Ganymede is expected to have a higher content of non-water materials, Callisto's crust is likely to contain more of such materials than Ganymede's due to the absence of the differentiation process. This will be important in future chapters, since the impurity content is the parameter that affects dielectric properties more than any other. In particular, if it is true that Callisto's crust has a lower amount of ice, attenuation is expected to be higher.

2.2 Surface composition

2.2.1 Ice characteristics

Like all the satellites orbiting around the outer gaseous planets, the Galilean ones (except for Io) have surfaces dominated by water ice. The purity of such ice decreases going from Europa to Callisto, as shown by the decreasing albedo. The absorption bands found in IR spectra that indicate the presence of water ice are those at 1.50, 1.57, 1.65, and 2.02 μm (Ligier et al., 2019c). The absorption bands of ice on Ganymede suggest that it is bound to a host molecule by weak hydrogen bonds, forming a hydrated material that, for example, could be $MgSO_4$, Na_2SO_4, or H_2SO_4 (Dalton et al., 2010; Pappalardo et al., 2004). As predictable, ice bands are stronger in the light (higher albedo) craters. On Callisto, water spectral features suggest that there are some patches of pure water ice, while some others are ice-free (Moore et al., 2004).
Ice is believed to be mostly amorphous on Europa, mostly crystalline on Callisto, and in both forms on Ganymede. This is due to the different processes competing to change the form in which ice is found: radiolysis and

sputtering tend to make it amorphous, while thermal annealing and recrystallization during the diurnal temperature cycle tend to make it crystalline (Dalton et al., 2010). Europa is closer to Jupiter and has a slightly lower surface temperature, therefore the first kind of processes dominate, while the opposite occurs on Callisto. On Ganymede, both forms are present, since its surface is partially protected by the intrinsic magnetic field, so that ice is mostly amorphous close to the magnetic poles (Dalton et al., 2010). On both, ice rapidly becomes crystalline under the surface and will, therefore, be assumed to be in such form in this work.
The grain size of ice on Ganymede should be between 0.1 and 1 mm, with higher values in the trailing equatorial, according to Pappalardo et al. (2004). Other authors suggests that the lower limit for the grain size is 1 μm (Stephan et al., 2017). They also claim that Callisto's ice has roughly the same grain size at the poles but slightly larger values at low latitudes. This could be due to the higher temperature that favors sublimation and crystal growth.

Abundance on Ganymede

The amount of water ice on Ganymede should be about halfway between Europa and Callisto, as can be inferred from the respective visible albedos. The spectra analyzed in Calvin et al. (1995) suggest that water ice represents 90 wt% of Ganymede's surface, as found by Clark (1980). The authors also claim that, differently from Callisto, there are nearly no areas that are ice-free. On the other hand, in Pappalardo et al. (2004) the authors suggest a much lower value of 50 - 60% of water ice, which could decrease to about 20% in the dark regions. According to Showman and Malhotra (1999), ice makes up from 50 to 90% of the mass at the surface. A more detailed study was carried out by Ligier et al. (2019c), with interesting results. They found a maximum abundance around 60% in some polar regions and a minimum of about 10% close to the trailing hemisphere apex at low latitudes. In general, ice abundance increases going from the equator to the poles.

Abundance on Callisto

Callisto is generally believed to have a lower amount of water than Ganymede ice on its surface. In Calvin et al. (1995) the authors claim that ice abundance ranges from 20 to 45 wt% on Callisto's surface, based on visible and infrared spectra (from 0.2 to 5 μm). They also point out that their result is in contrast with previous work (Clark et al., 1986), according to which the abundance can reach 70%. Previously, it had been estimated that the amount of ice on Callisto's surface could be between 30 and 90 wt% (Clark, 1980). The first cited work better agrees with Showman and Malhotra (1999), according to which ice represents at most 50% of the surface. A

completely different result has been obtained by Ligier et al. (2020), where the authors claim that the abundance of ice is $\leq 10\%$.

2.2.2 Impurities

The impurities found on the surfaces of the Galilean satellites have not uniquely identified yet. The presence of materials is mainly studied using albedo data and spectra from the UV to the NIR range. Table 2.1 shows some of the compounds identified on the surfaces of all the Galilean satellites, and those predicted to exist there. The table is taken from Dalton (2010), which represents a good summary of many previous works on this subject. The materials found in the last column have been predicted based on theoretical considerations, laboratory experiment, and tentative identifications (Dalton, 2010).

Planet	Satellite	Temperature	Known Compounds	Expected Compounds
Jupiter	Io	80–130 K; 150–200 K at hot spots; peaks of 400–1870 K	SO_2, H_2S, H_2O, silicates	S_2O, S_8, S_nO, Mg-rich orthopyroxene
	Europa	86–132 K	H_2O, SO_2, CO_2, H_2O_2, O_2, hydrates of H_2SO_4, $MgSO_4$ and Na_2SO_4	heavily hydrated and/or hydroxylated minerals, tholins
	Ganymede	90–160 K	H_2O, SO_2, CO_2, O_2, O_3	Aliphatic hydrocarbons, heavily hydrated and/or hydroxylated minerals, tholins
	Callisto	80–158 K	H_2O, SO_2, CO_2, O_2, silicates	Aliphatic hydrocarbons, heavily hydrated and/or hydroxylated minerals, tholins

Figure 2.1: Surface temperatures of the Galilean satellites, and compounds known or expected to be present on their surfaces (Dalton, 2010).

Other compounds expected to be found include carbonic acid (H_2CO_3) and hydrogen cyanide (HCN) (Dalton et al., 2010). In Calvin et al. (1995), several works estimating the kind of chemical impurities on the Galilean satellites are mentioned. The authors cite ozone, oxygen ions, hydrogen peroxide and molecular oxygen for Ganymede. Based on visible and IR spectra, it has been claimed that Fe- and Mg-end member serpentines must be present on Callisto (Calvin and Clark, 1991). Such materials are similar to those found inside carbonaceous chondrites. Ammoniated clays have been proposed as a possible contaminant by Calvin and Clark (1993), and this is agreement with theoretical formation models. Based on the analysis of several craters of Ganymede's surface with different dimensions, it has been found that the dark material should be the same for all craters and that it is too bright to have the same composition as asteroids of type C and D (Helfenstein et al., 1997). The same result has been obtained by

other authors (Schenk and McKinnon, 1991), and they also pointed out that asteroids of types A, E, Q, S, and V are too bright for Ganymede's craters. Other possible molecules for Callisto are listed in Moore et al. (2004), and these include methylidyne radical-bearing compounds and cyanide. They also point out that some molecules like SO_2 would evaporate at the surface conditions found here, so they should be bound to other host molecules to remain stable.
The next question that could be asked is where these substances come from. Many compounds can be originated thanks to the strong volcanic activity on Io. This body also has a low gravity and almost no atmosphere, so that the materials emitted by the volcanoes can escape and reach the other satellites. In this way, oxygen, sulfur, sodium, potassium, and chlorine (Dalton et al., 2010) are believed to form new compounds on the surfaces of Ganymede and Callisto. What's more, at least some of the sulfur on Ganymede is believed to have an endogenous origin. In particular, the core is believed to be a mixture of Fe and FeS (Kimura et al., 2009; Vance et al., 2014; Sotin et al., 2020), and therefore some material could have reached the surface in the past, when the body was hotter and more tidally active. In the end, materials are also brought by impactors. For this reason, several authors proposed a carbonaceous chondrite-like composition in their works (e.g., Dalton et al. (2010); Sotin et al. (2020)).

2.3 Internal composition

It is important to separate the surface composition from the internal one, since the two are in principle different. Because of what said about the differentiation process, it is expectable that the surface composition of Callisto resembles the total composition more than in the case of Ganymede. One of the first estimates was based on thermal models and density arguments (Consolmagno and Lewis, 1976). For Callisto, the authors assume ferromagnesium silicates as non-water components and the resulting abundance is 40 wt%. For Ganymede, the resulting abundance is 60% in the case of high density (3.7 g/cm^3) silicates and 80% in the case of low density (2.5 g/cm^3) silicates. However, these estimates are biased by the assumed values of the average densities of the two bodies. They assume a density of 2 g/cm^3 for Ganymede which is rather close to the modern value, but they assume a density of 1.4 g/cm^3 for Callisto, which is about $\sim 24\%$ lower than today's value. The same authors (Consolmagno and Lewis, 1977) made more estimates based again on thermal modeling, finding the same result for Callisto. For Ganymede, they found a slightly different abundances, that is from 65% to 85%. Later on, some interior models for Ganymede and Callisto were built based on the assumptions that they are both differentiated into three layers, and that the rocky component has the same composition of CI car-

bonaceous chondrites (Mueller and McKinnon, 1988). The authors found that both satellites have a silicate volume fraction lower than 60%. However, as already discussed, today we know that Callisto is, at most, only partially differentiated. This estimate must therefore be considered with caution. Subsequently, a rock abundance between 54 and 59 wt% for Ganymede has been obtained based on the results of differentiation of a system of H_2O, $MgSO_4$, and $NaSO_4$ plus inert rock (Kargel, 1991). This model implies the presence of Mg and Na sulfates on the surface due to cryovolcanism, and the presence of these kinds of substances has been confirmed by the observation, as discussed in the previous section. Another internal model with six different layers has been constructed assuming a rocky component with the same composition as L/LL type chondrites (density around 3.6 g/cm^3) (Kuskov and Kronrod, 2005). The resulting rock abundance ranges from 45 to 54 wt%. Based on the assumption that Callisto is partially differentiated and that convection occurs in its ice I crust, it has been claimed that the rock fraction in the said crust must be lower than 10 wt%, otherwise, the density of the crust would be higher than that of the below ocean and the structure would be unstable (McKinnon, 2006). A more recent estimate was made using numerical simulations of the thermal history of the two satellites, constraining the results thanks to the average bulk density and the normalized moments of inertia (Kimura and Kuramoto, 2011). The result is that the amount of hydrated silicates must be between 40 and 55 wt%, with a higher value for Ganymede than for Callisto. In particular, they find that if the silicates were more abundant than 55 wt%, both satellites would be totally differentiated, while it has already been shown that Callisto cannot be in such a state. On the other hand, an abundance lower than 40% would imply an undifferentiated Ganymede, which is also unrealistic.

Chapter 3

Physical models from the literature

3.1 Thermal gradients and surface temperature

Surface temperature is probably the best-constrained parameter that will be discussed in this work. However, this is only the starting point, since a temperature profile inside the crust has to be assumed. The surface temperature naturally decreases going from the equator to the poles. It also varies locally due to the variation of thermal inertia, which is a consequence of the different chemical compositions (Pappalardo et al., 2004).

3.1.1 Surface temperature of Ganymede

It has been tried to estimate the heat flux at the moment of formation of Ganymede's dark terrains, using an average value for the surface temperature of 120 K (Nimmo and Pappalardo, 2004). This falls exactly in the middle of the temperature range shown by Pappalardo et al. (2004), that is from 90 to 150 K. In their modeling, Vance et al. (2014) used a surface temperature of 110 K. They also assume that the temperature at the bottom of the H_2O layer (including the putative ocean) reaches 280 K. Using infrared spectra, Ligier et al. (2019c) tried to fit the 1.65 μm absorption band of water ice, finding an average temperature of 125 ± 25 K for the ice-rich areas (bright craters and trailing hemisphere). Discussing the possible grain size of ice, it has been assumed a maximum diurnal temperature of 150 K at the equator and 80 K at the poles (Stephan et al., 2017). A study carried out to determine the ice shell structure of Ganymede and Callisto through the analysis of impact craters showed that the best fit to the observed crater radii-impactors size relation implies a surface temperature of 120 K and a thickness for the conductive crust of 12 km (Bjonnes et al., 2018). In a similar study, a surface temperature of 110 K has been used to explain the

formation of Ganymede's grooved terrains (Hammond and Barr, 2013).

3.1.2 Surface temperature of Callisto

According to Moore et al. (2004), the surface temperature of Callisto ranges from the 165 K in the subsolar region to the 80 K of the predawn equatorial nighttime. They also claim that the dark component is, on average, hotter than ice. The temperature at the poles should be similar to that of Ganymede but, at the equator, the temperature is higher (165 K) on Callisto (Stephan et al., 2017).

3.1.3 Thermal gradients

Once the value of the surface temperature has been fixed, it is important to determine how this quantity changes inside the body. In planetary bodies, two heat transfer mechanisms can occur: conduction and convection. As far as the inner planets are concerned, Earth is the only one presently losing heat via convection (volcanism). For such a process to occur, the body must have a thin lithosphere and a high amount of stored heat. The Earth accumulated heat thanks to accretion, differentiation, and radiogenic decay. Small-sized bodies, such as Mercury or the Moon, only experienced convection in the very early stages of their lives, because they rapidly lose most of their internal heat. The amount of heat stored is proportional to the total volume of the body, while the heat loss is proportional to its total surface, therefore the rapidity at which it loses heat is $\propto 1/R$, with R radius.
Since Ganymede and Callisto have approximately the size of Mercury, and are much colder, they are, in principle, unlikely to have experienced convection. On the other hand, they are also subject to tidal forces driven by the great mass of Jupiter and by the Laplace resonance. Schubert et al. (1981) stated that radiogenic decay cannot have caused convection in the early stages of the lives of these bodies, so the same holds in the present day, since this form of energy decreases over time. They also claim that accretional heating could have caused melting (which favors convection) only in the outer layers of Ganymede. Conversely, Hammond and Barr (2013) assumed solid-state convection as a way to explain the formation of Ganymede's grooved terrains. However, these terrains formed some time ago and this assumption may not be valid at the present day. As pointed out by McKinnon (2005), convection would increase radar attenuation, since the temperature would be much higher. However, as already said, attenuation would be comparable to the conductive case in the cold downwellings. In any case, in the literature, the majority of the authors (e.g., Bjonnes et al. (2018); Kuskov and Kronrod (2005)) now assume that heat is transported via conduction inside Ganymede and Callisto, while convection is thought to occur inside Europa (e.g., McKinnon (2004)).

As known by thermodynamics, heat spontaneously flows from hotter to colder bodies. If two objects with different temperatures are in contact, heat can flow through conduction. This mechanism is due to the collisions between molecules, which occur because of the internal energy of the body. In practice, inside a solid, there are atoms, molecules, and electrons continuously rotating and vibrating. Therefore, they hit each other and exchange energy. In the case of planets and satellites, the two "bodies" touching each other are the spherical layers with temperature decreasing from the center outward. Heat transfer by conduction is regulated by Fourier's law

$$q = -k\frac{dT}{dz}, \tag{3.1}$$

with q local heat flux density ($\mathrm{W/m^2}$), k is the thermal conductivity of the material, and $\frac{dT}{dz}$ is the temperature gradient perpendicular to the area through which heat flows. The negative sign accounts for the fact that heat flows from bodies at higher temperatures towards those at lower temperatures. A simple solution for the conductive ice shell of a satellite, like Ganymede or Callisto, can be found by assuming k constant and $q \approx 0$, which give

$$T(z) = T_s + (T_b - T_s)\frac{z}{b}, \tag{3.2}$$

with T_s surface temperature, b shell thickness and T_b temperature at such base (Chyba et al., 1998). However, the thermal conductivity is, in general, temperature-dependent but, for some materials, it can be assumed to be constant over a limited temperature range. For ice, at low temperatures, it can be assumed to be $k(T) \simeq a/T$ (Chyba et al., 1998) with a given constant. What's more, q is not exactly zero, since there is at least radiogenic decay that provides a certain amount of heat. In general, it can depend on temperature itself (for example in the case of tidal heating) but, in this case, can still be taken to be constant. Using $k = a/T$ and $q \neq 0$ (constant) yields a temperature profile in the form

$$T(z) = T_s e^{z/h}, \tag{3.3}$$

with $h = a/q$ being the scale height (Chyba et al., 1998). Here, for simplicity, the temperature gradient will be assumed to be linear. Some values of the thermal gradients are shown in table 3.1.

3.2 Porosity gradients

Porosity is the least influential when it comes to calculating the dielectric permittivity. Nevertheless, it is important to fix a value for this quantity and, possibly, an internal gradient as done for the temperature. Porosity is

Author	Gradient
Lewis (1971)	1 K/km
Heggy et al. (2017)	2 K/km
Bjonnes et al. (2018)	5 and 10 K/km

Table 3.1: Thermal gradients assumed for the Galilean satellites in the literature.

defined as the measure of the void spaces in a material, and is the fraction of the volume of voids over the total volume, between 0 and 1. On icy satellites, porosity may result, for example, from geological activity (e.g., cracking due to tidal heating) or impacts. If high, it can affect radar penetration. This quantity is, in general, thought to decrease with depth, due to several mechanisms (e.g., mechanical compaction or thermal modification). Despite that, low thermal gradients like those expected for Ganymede or Callisto would only allow a small porosity gradient (Heggy et al., 2017). Byrne et al. (2018) claim that, based on the expected pressure in the interior, porosity should rapidly drop to zero at a depth of a few hundred meters. Their claim is, in turn, base on the model by Vance et al. (2014). Das and Mukherjee (2020) contains an up-to-date review of several porosity-depth models. The classical one is the Athy relation

$$\phi(z) = \phi_0 e^{-cz} \tag{3.4}$$

with $\phi(z)$ being the porosity at depth z, ϕ_0 porosity at the surface, and c is a constant called compaction coefficient. This formula, and all the other found in the cited work, are based on studies of Earth rocks. However, it may be possible that these models can be adjusted to work on icy satellites as well. If this were the case, an exponential decrease as the one shown would justify the rapid drop of porosity with depth.

Croft (1993) constructed models relating the mean densities and the radii of several icy satellites. He claims that porosity should be an important factor affecting the density and the moment of inertia of small- and mid-sized satellites. In practice, according to such a model, large bodies like Ganymede and Callisto, have very low porosities. This is an opinion shared by Eluszkiewicz and Leliwa-Kopystynski (1988), based on theoretical models relating poros-

ity and moment of inertia. Based on laboratory results, McKinnon and Parmentier (1986) stated that porosity inside Ganymede and Callisto could be as high as 40%. Ostro and Shoemaker (1990) pointed out that the crater distributions of Ganymede and Callisto are similar to that of the Moon, and this may imply a similarity between the respective regoliths. They report a 45% porosity value for the Moon's surface (decreasing downward), but they also underline that the Moon is mostly made up of silicates, while Ganymede and Callisto have substantial amounts of ice (and their densities are much lower). More recently, for a dielectric modeling of Ganymede and Callisto, Di Paolo et al. (2018) used a constant 10% porosity, as previously suggested by Heggy et al. (2017).

3.3 Chemical impurities gradients

The chemical composition of Ganymede and Callisto has been widely discussed in the previous chapter. As said, the surface composition does not necessarily reflect the overall one, especially in the case of Ganymede, due to the differentiation process. Another fact that has already been mentioned is that Ganymede's surface consists of dark and light terrains, which display different chemical compositions. Since RIME will be able to penetrate at least a few kilometers inside the ice, it is necessary to assume a gradient for the impurity content. This will be the most influential factor in determining the dielectric properties of the medium. In general, the gradient should be negative. This is justified by the fact that the surface contains more impurities than the interior because of the origin of such compounds. They may come from meteoric impacts, from Jupiter's magnetosphere, from Io's eruptions or cryovolcanic activity. In any case, all these processes only affect the most surficial layers. It could be argued that, in the previous chapter, it has been stated that both bodies have internal layers denser, and therefore impurity-richer, than the outer ones, especially in the case of the differentiated Ganymede. However, this is more a "large scale" effect, meaning that, of course, Ganymede's core is denser than its crust, but RIME will not penetrate over the crust and reach the mantle nor the nucleus. Therefore, the impurities found in the outer kilometers of Ganymede are mostly found very close to the surface, while the rest of the crust consists of a cleaner ice. Callisto is in a slightly different situation, since it is less, if at all, differentiated. To account for this fact, the overall impurity content will be assumed to be higher, but still decreasing with depth.
An interesting gradient for the amount of chemical impurities is the one proposed by Heggy et al. (2017). The authors assumed a gaussian decreasing dust mass fraction profile for all cases. The surface values are different for each case, and they are 20% dust mass fraction for Ganymede's bright terrains, 55% for Ganymede's dark terrain, and 65% for Callisto. The gradients

are shown in Figure 3.1.

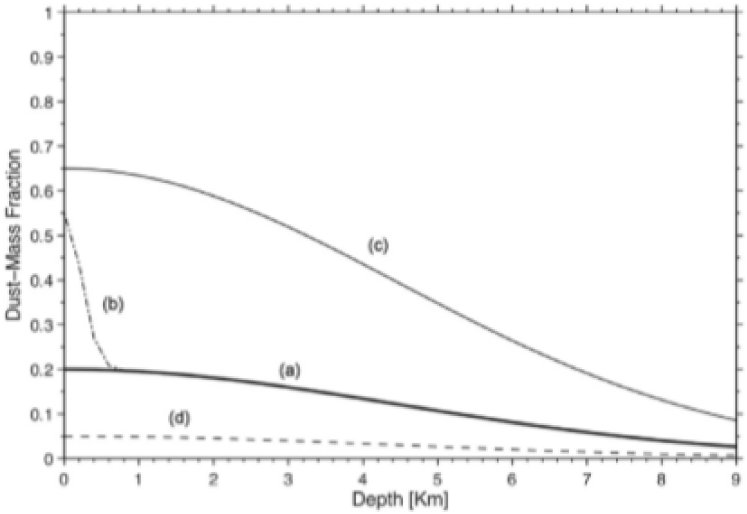

Figure 3.1: Dust mass fraction gradients inside Ganymede (plot a for bright terrains and b for dark terrains), Callisto (plot c) and Europa (plot d) (Heggy et al., 2017).

As shown, these gradients are consistent with the qualitative arguments presented above.

3.4 Dielectric permittivity

Dielectric permittivity has already been defined in the first chapter. Now it is important to show how this quantity depends on the three parameters discussed before: temperature, porosity, and impurity content. The frequency may not be strictly important since, as already said, dielectric permittivity is frequency-independent in the 1 MHz - 10 GHz range for pure water ice (Brouet et al., 2016).

3.4.1 Temperature dependence

In Chapter 1, the formulas for the attenuation and the dielectric permittivity (real and imaginary part) have been shown. These are equations 1.5 and 1.8, respectively. How do these quantities depend on temperature? As shown, the dielectric permittivity depends on the relaxation time, which has already been defined. It can be expressed as a function of temperature

$$\tau = C \exp\left[\frac{E}{k_B T}\right], \tag{3.5}$$

where C is a constant that depends on the material considered, $E = 0.571$ eV is the activation energy, k_B is the Boltzmann constant and T is the temperature. This temperature dependence is justified by the fact that the higher is the temperature and the stronger is thermal agitation that opposes to the ordered orientation that polarization causes. What's more, the Curie-Weiss law gives

$$\varepsilon_s - \varepsilon_\infty = \frac{A}{T - T_c} \tag{3.6}$$

with A constant that depends on temperature and frequency, T is again the absolute temperature, and $T_C \simeq 35$ K the Curie temperature. Finally, the high-frequency permittivity ε_∞ increases linearly with temperature as

$$\varepsilon_\infty = 3.02 + 6.41 \times 10^{-4} T \text{ (Chyba et al., 1998).} \tag{3.7}$$

It is important to note that these dependencies appear in the attenuation formula, since it depends explicitly on the square root of the real dielectric permittivity and the loss tangent. Figure 3.2 shows the temperature dependence of attenuation for different ices.

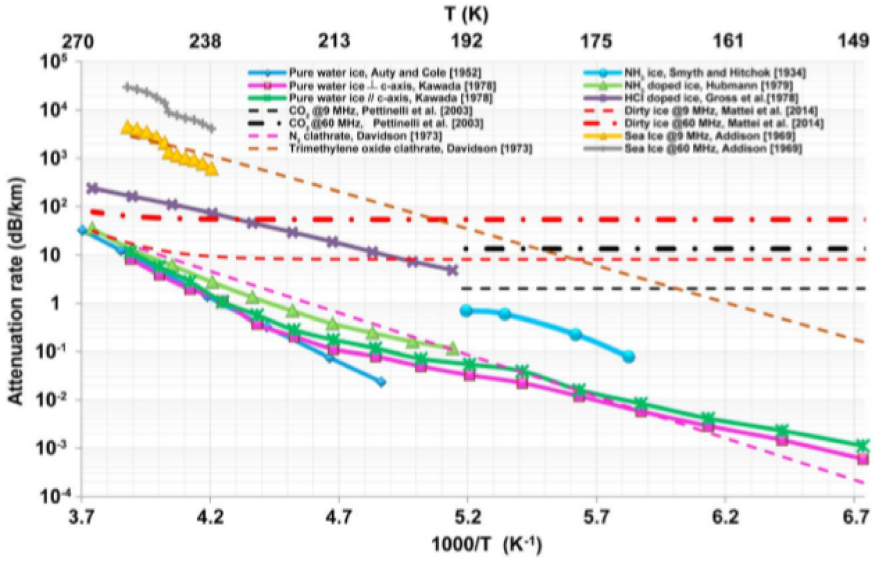

Figure 3.2: Attenuation as a function of temperature for different ices taken from Pettinelli et al. (2015). The references for the data sets are included in the figure. When not specified, the data at 9 and 60 MHz coincide.

3.4.2 Porosity dependence

Porosity affects the dielectric properties because it introduces some voids inside an otherwise homogenous medium. Recent laboratory measurements

were performed by Brouet et al. (2016). They measured the real dielectric permittivity of ice and ice-dust mixtures over a wide frequency (50 MHz - 2 GHz) and porosity (31% - 91%) range. They find that the real part of the permittivity increases with the increasing bulk density and decreases with increasing porosity. Fitting the data, they find a relationship in the form

$$\varepsilon' = E^{1-\phi}, \tag{3.8}$$

with ϕ porosity and $E = (\varepsilon'_D/\varepsilon'_I)^{V_D} \times \varepsilon'_I$, where ε'_I is the real dielectric permittivity of pure ice, ε'_D is that of pure dust, and V_D the volumetric dust fraction. As a consequence, the parameter E increases with increasing dust fraction. The value found for pure ice is at $\phi = 0$ is consistent with the expected dielectric permittivity of pure water ice. They also propose the empirical relation

$$\varepsilon'(F_D, \phi) = \left(5.65 \times F_D^2 - 0.23 \times F_D + 3.22\right)^{1-\phi} \tag{3.9}$$

which explicitly depends on the dust mass fraction F_D. Figure 3.3 shows their data for the real permittivity and the fitting curves.

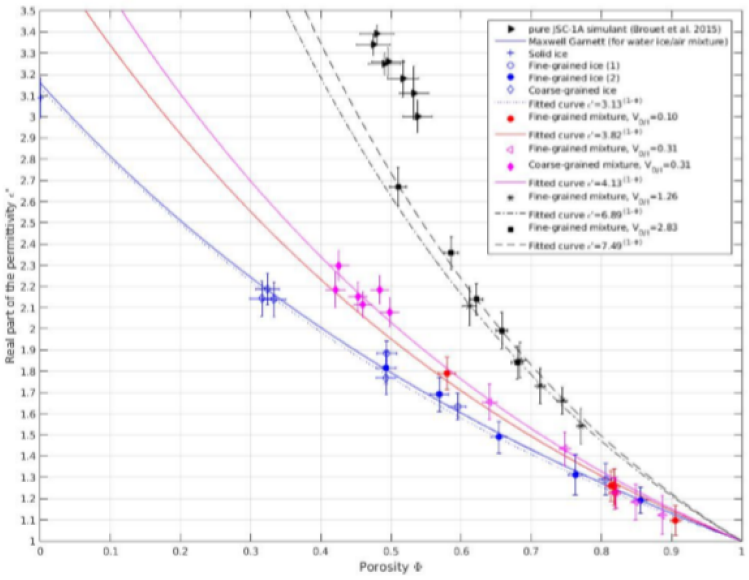

Figure 3.3: Real dielectric permittivity as a function of porosity taken from Brouet et al. (2016). The reported values have been averaged over frequency in the range 50 MHz - 2 GHz.

The authors claim that these results can be extended on a broader frequency range, down to 10 MHz. As said, the central frequency of RIME is 9 MHz, so what shown can be used here with a certain degree of confidence.

3.4.3 Impurity content dependence

Unfortunately, attenuation is strongly increased by the presence of non-ice compounds. The dielectric permittivity resulting from the insertion of N different impurities into a porous ice matrix is given by the Rayleigh multiphase mixing formula

$$\varepsilon_{eff} = \varepsilon_e + 3\varepsilon_e \frac{\sum_{n=1}^{N} f_n \frac{\varepsilon_{i,n}-\varepsilon_e}{\varepsilon_{i,n}+2\varepsilon_e}}{1-\sum_{n=1}^{N} f_n \frac{\varepsilon_{i,n}-\varepsilon_e}{\varepsilon_{i,n}+2\varepsilon_e}}, \tag{3.10}$$

which is valid for spherical scatterers of permittivities $\varepsilon_{i,n}$ in a medium with permittivity ε_e. Here, f_n is the n-th mass-fraction of the inclusions of the n-th phase of the mixture. The background medium is water ice. The different contaminants assumed will be shown in Chapter 4. The abundances will be based on the arguments shown in Section 3.3 and in Chapter 2.

Chapter 4

Scenarios and results

4.1 Methods

The main purpose of this work is to evaluate how deep the RIME signal can travel through the crusts of Ganymede and Callisto. Quantitatively, this is done by calculating the cumulative attenuation. In equation 1.8, three quantities determine ice attenuation for an electromagnetic wave: the frequency of the signal, the real, and the imaginary permittivity of the ice itself. The real permittivity is frequency-independent in the part of the spectrum under consideration, while the imaginary part is in the form $\varepsilon'' \propto \nu^{-1}$. What's more, the imaginary permittivity strongly depends on temperature, and so does attenuation. Figure 4.1 shows that attenuation increases by several orders of magnitude over the temperature range 95 - 273 K. Since temperature increases at depth inside planetary bodies, the same will be true for the imaginary permittivity of the ice that makes up such bodies. Therefore, a temperature profile $T(z)$ (z being the vertical coordinate) will result in a $\varepsilon''(z)$ profile. Substituting this into equation 1.8 leads to the attenuation profile $A_{\mathrm{dB/km}}(z)$. It is now possible to define the cumulative attenuation as

$$A_{\mathrm{dB}}(z) = 2 \int_0^z A_{\mathrm{dB/km}}(z')\, dz'. \tag{4.1}$$

This is the attenuation profile integrated over the distance traveled by the radar signal twice (since such signal goes down and then returns to the receiver). As follows from the above explanation, this quantity only depends on the frequency of the signal (which is fixed), and from the temperature profile. Of course, as explained in the previous chapter, this is true for pure water ice but the presence of impurities and porosity alters the resulting attenuation.
As reported by several authors (e.g., Blankenship et al. (2009) and Heggy et al. (2017)), the detectability limit of an instrument like RIME in the

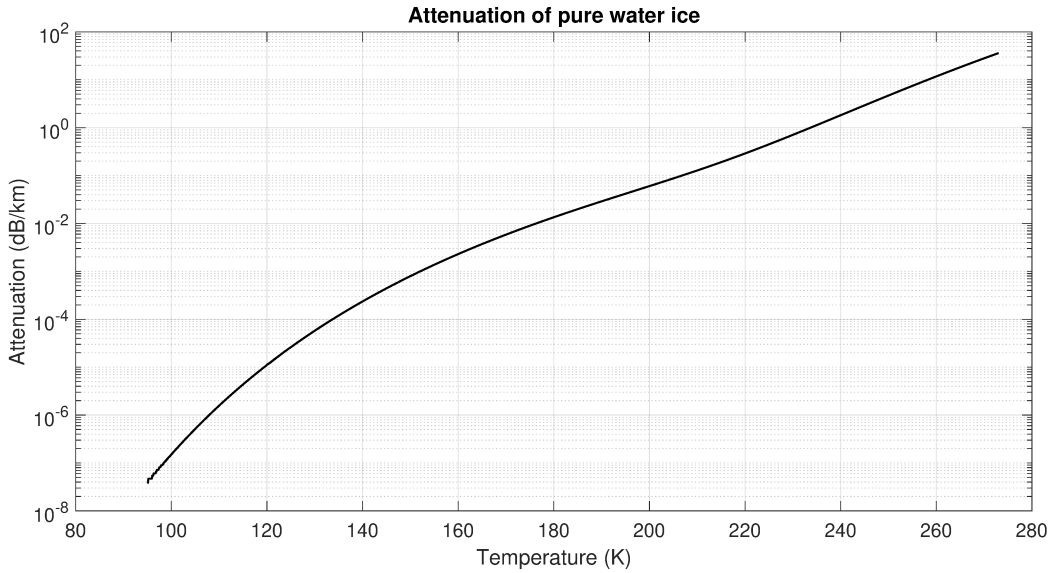

Figure 4.1: Attenuation for pure water ice as a function of temperature. The temperature range is 95 - 273 K. Data taken from Kawada (1978).

Jovian system should correspond to a cumulative attenuation of 55 dB due to several noise sources (see Blankenship et al. (2009) for details). Therefore, this is the observational limit that will be assumed here. In every figure, when the resulting cumulative attenuation reaches such a limit, it will be shown as a black dashed line.

4.2 Space of variables

In this section, I describe the values used for each of the variables relevant to the model, and why such values were used. All the simulations were run to a depth of 13 km with a sampling of 10 m. Bruzzone et al. (2013) stated that the expected depth that can be probed by RIME is smaller, around 9 km, but it can be useful to go further with the models and see what the situation could be deeper inside these bodies.

4.2.1 Surface temperature and thermal gradient

The estimates for the surface temperature of Ganymede and Callisto have been described in the previous chapter. This quantity ranges from about 80 K to 150 K for Ganymede, and 165 K for Callisto. However, it is important to note that this quantity is merely relevant to the aim of this work, which is the total radar attenuation. In particular, the permittivities of the different contaminants have been assumed to be temperature independent, so the

effect of temperature is only visible through the increase in the imaginary permittivity of the water ice component, especially at $T > 200$ K, as shown in the previous section. Therefore, what can affect the total attenuation is the thermal gradient, if high. The surface temperature could be important if it was assumed to be very high (e.g., 160 K) but, with a low thermal gradient, the increase in the water ice attenuation still would not be visible. Moreover, the results obtained with such a high temperature could be realistic only for observations at the equator of Callisto. Therefore, the surface temperature has here been fixed at 120 K, which represents an average value for both Ganymede and Callisto, as also suggested by Heggy et al. (2017).
As shown in the previous chapter, the thermal gradient of these bodies is not tightly constrained. Table 3.1 shows the thermal gradients found in the literature, assuming that heat is transported via conduction. For the sake of completeness, in this work, all the four values reported in the table have been used. They are shown in Figure 4.2.

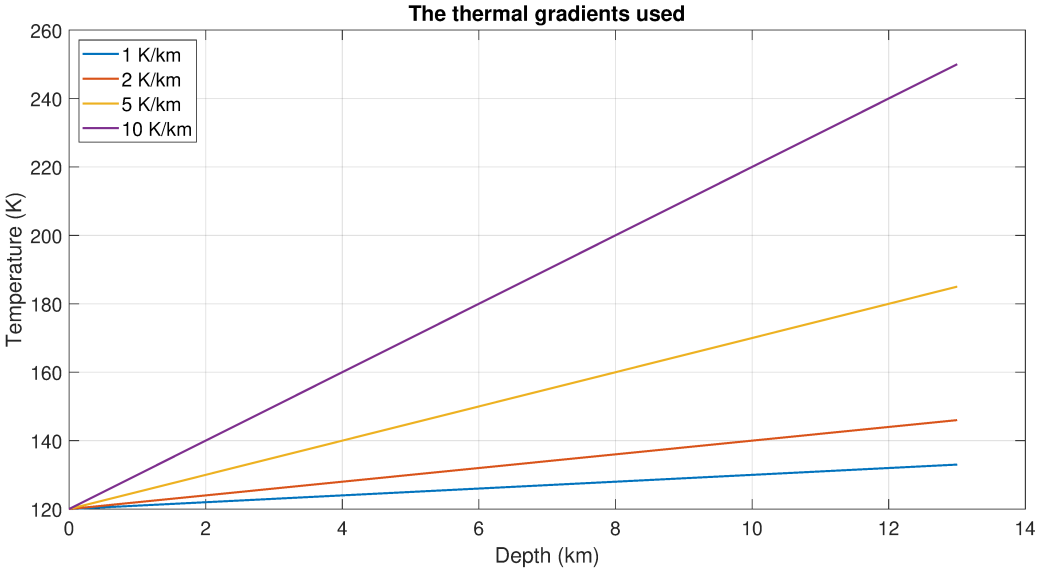

Figure 4.2: The four thermal gradients used in the simulations.

It is important to note that not all these gradients are equally likely to be representative of Ganymede and Callisto. In their work, Bjonnes et al. (2018) ran simulations with gradients of 5 and 10 K/km to reproduce the observed features of the craters found on these satellites. However, such craters formed at some point in the past. This means that these two thermal gradients might be realistic for the distant past of Ganymede and Callisto, when both bodies were hotter. Today, the actual gradient is likely to be closer to the value of 2 K/km used by Heggy et al. (2017). Therefore, the values taken from Bjonnes et al. (2018) will be used only as a comparison,

and the 10 K/km-case will be treated as a "worst case scenario".

4.2.2 Porosity

In Section 3.2, the possible values for porosity from the literature have been discussed. However, the reported values are rather different from one another. To explore all the different possibilities, in this work, the porosity has been varied. In particular, the values used are 0%, 15%, 30%, and 45%. In every case, it has been assumed to be constant with depth, as done, for example, by Heggy et al. (2017). As stated, the highest porosity possible according to the literature is 40-45%, and this is why higher values have not been used. What's more, if it is true that this quantity rapidly goes to zero below the surface, its effect is so small that it can simply be assumed to be zero, since a porosity different from zero only for a few hundred meters is not very important when integrating over 13 km as in this case. The 15% and 30% cases have been used as intermediate values in the 0-45% range. As for the thermal gradients, not all the values of porosity are equally likely. The 45% value is unrealistically high, and will be considered only as a "best-case scenario" (since such a high value could significantly lower attenuation).

4.2.3 Impurity content profile

The chemical impurities profiles used here are similar to the ones reported in Section 3.3, taken from Heggy et al. (2017). The surface values assumed (20% for Ganymede's bright terrains, 55% for Ganymede's dark terrains, and 65% for Callisto) are consistent with what is described in Chapter 2. As said, these profiles have a gaussian behavior, and the assumed standard deviation is 4.5 km. The profile for Ganymede's dark terrains is the same as for the bright terrains, with the insertion of an impurities-rich layer at the surface. Here, the chemical gradient is linear and ends at a depth of 1 km. Both gradients used for Ganymede are shown in Figure 4.3. In addition to these, other three profiles have been used for comparison purposes:

- The first one is a zero-impurity profile so that the results refer to porous pure ice. This is physically unrealistic, especially for Callisto or the dark terrains of Ganymede, but the comparison between this case and the other ones accounting for the presence of impurities better explains the effect of the non-ice component on the attenuation.
- The second one is a horizontal profile so that the impurities content is constant with depth, fixed to 65% as for Callisto. This is also unrealistic but, similarly to what said for the 10 K/km thermal gradient, it will be treated as a worst-case scenario.
- The last one is a profile with the same surface value as Callisto, but with a standard deviation of 9 km. This case is rather interesting

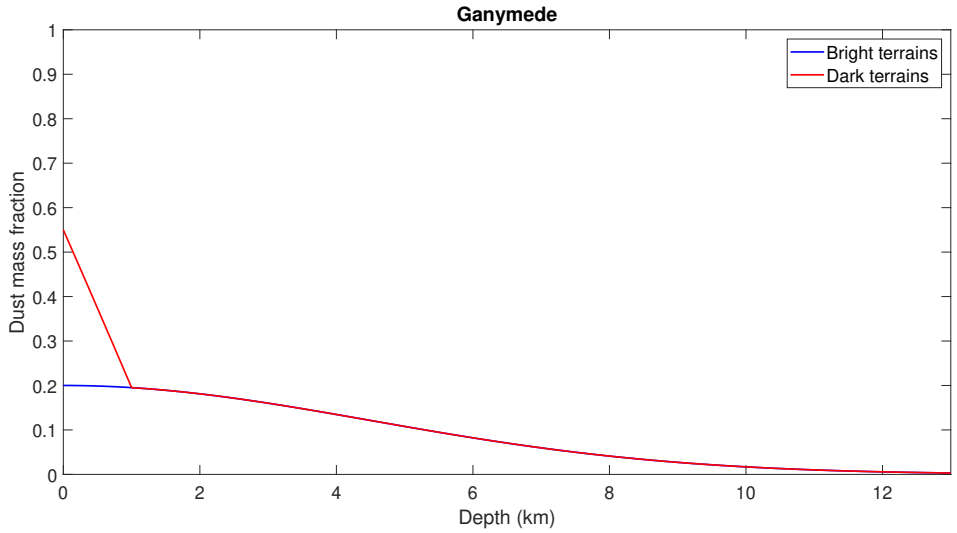

Figure 4.3: The impurity-content profiles assumed for the bright and dark terrains of Ganymede.

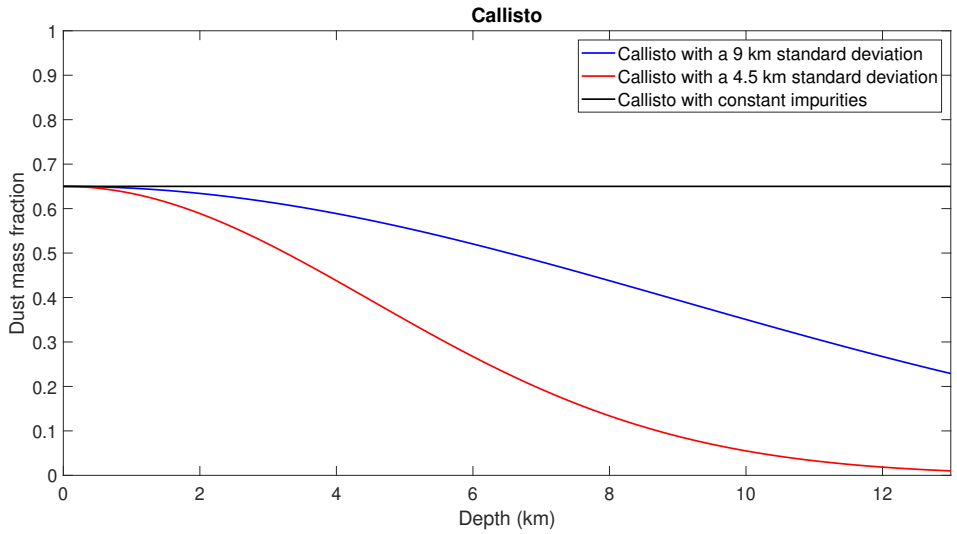

Figure 4.4: The three impurity-content profiles assumed for Callisto.

because of what said about the lack of differentiation inside this body. Therefore, the use of a greater standard deviation can account for this fact, since it implies a slower decrease of the dust content with depth.

The three gradients assumed for Callisto are shown in Figure 4.4.

4.2.4 Dielectric properties of silicate contaminants

Once chosen the profile of the impurity content, it is important to choose a proper contaminant. Here, three different contaminants from the literature have been used, and are shown in Table 4.1. All these contaminants are

Author	Name	Permittivity
Nunes and Phillips (2006)	Shergottite	8.8 + 0.017i
Heggy et al. (2012)	LL5 meteoric sample (MAC 88122)	7.2 + 0.033i
Heggy et al. (2012)	H5 meteoric sample (LEW 85320)	9.0 + 0.204i

Table 4.1: Different contaminants assumed for both Ganymede and Callisto from the literature. The H5 and LL5 values have been reported by Herique et al. (2018), and subsequently corrected for porosity using an inverse Rayleigh mixing formula.

meteoric since this kind of composition is expected to be similar to the one present in the outer icy satellites (e.g., Heggy et al. (2017)). The first one is the shergottite, which is the most common type of martian meteorite. The second belongs to the LL chondrites, which is a group of stony meteorites, the least abundant group of the ordinary chondrites, that contain a low amount of metal ($\sim 3.6\%$). The third one belongs to the H type ordinary chondrites, which are the most common type of meteorite and are very metal-rich ($\sim 9.6\%$).
The property that mostly affects attenuation is the imaginary permittivity of the contaminant, while the real part is less important. The shergottite sample has the lowest value of this quantity among the three, therefore the models with such contaminants are expected to have a lower attenuation (once the other parameters are fixed). The strongest attenuation is expected for the H5 sample, which is the richest one in metal. Naturally, the effect will be stronger when the impurity content is higher.

4.3 Simulations and results

4.3.1 Scenarios

Here are summarised all the results obtained using the different impurities profiles and the different contaminants. Each figure contains four plots, each one corresponding to a different thermal gradient, in which there are four different curves, each one corresponding to a different porosity value (as explained in the respective legends). Figures 4.5, 4.6, and 4.7 regard Ganymede's bright terrains, while the results for the dark terrains are shown in Figures 4.8, 4.9, and 4.10.

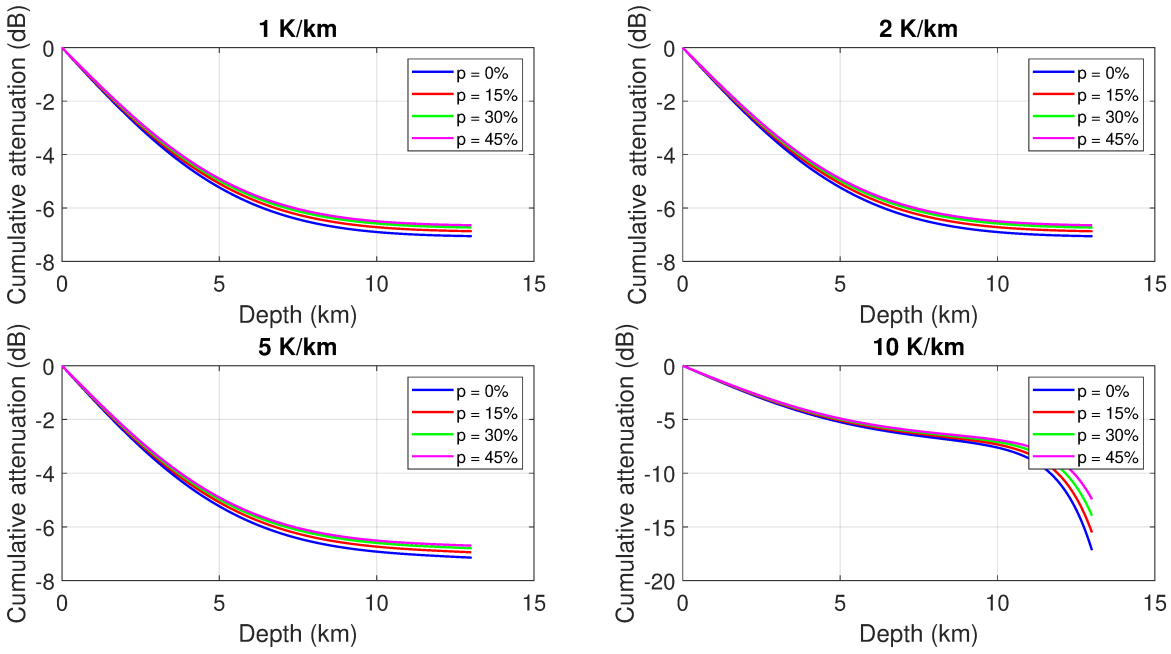

Figure 4.5: Cumulative attenuation in the case of Ganymede's bright terrains with the shergottite contaminant.

The results for Callisto are shown in Figures 4.11, 4.12, and 4.13 for the case with a 4.5 km standard deviation, Figures 4.14, 4.15, and 4.16 for the case with a 9 km standard deviation, and Figures 4.17, 4.18, and 4.19 for the case with constant impurities.

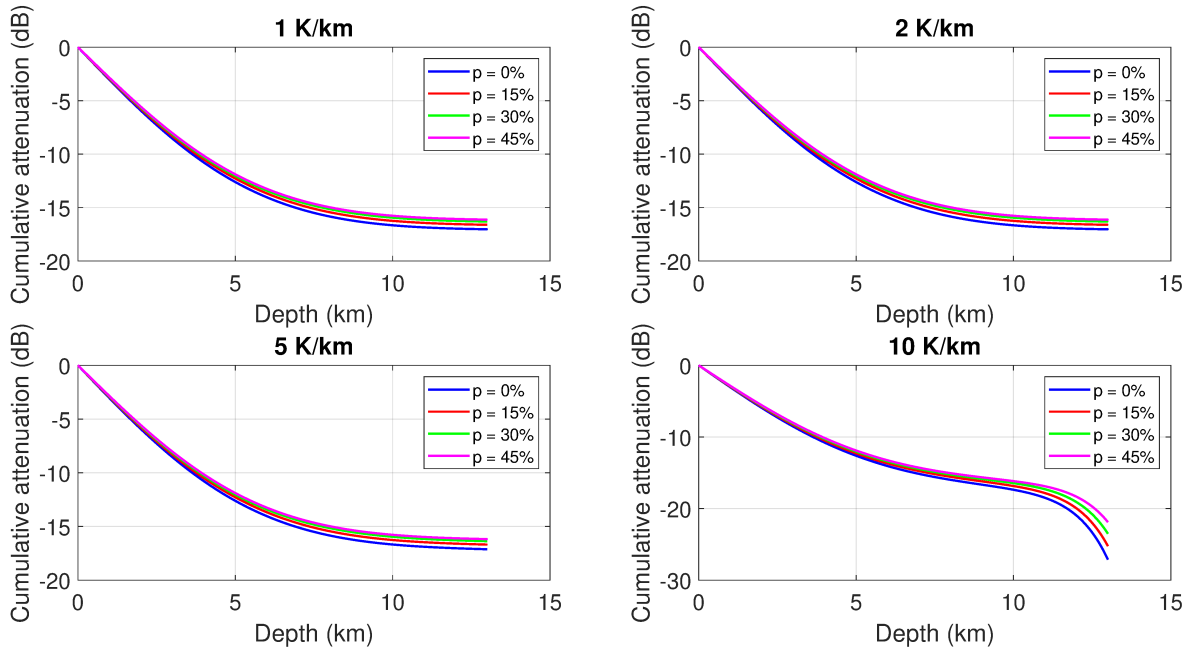

Figure 4.6: Cumulative attenuation in the case of Ganymede's bright terrains with the LL5 meteoric contaminant.

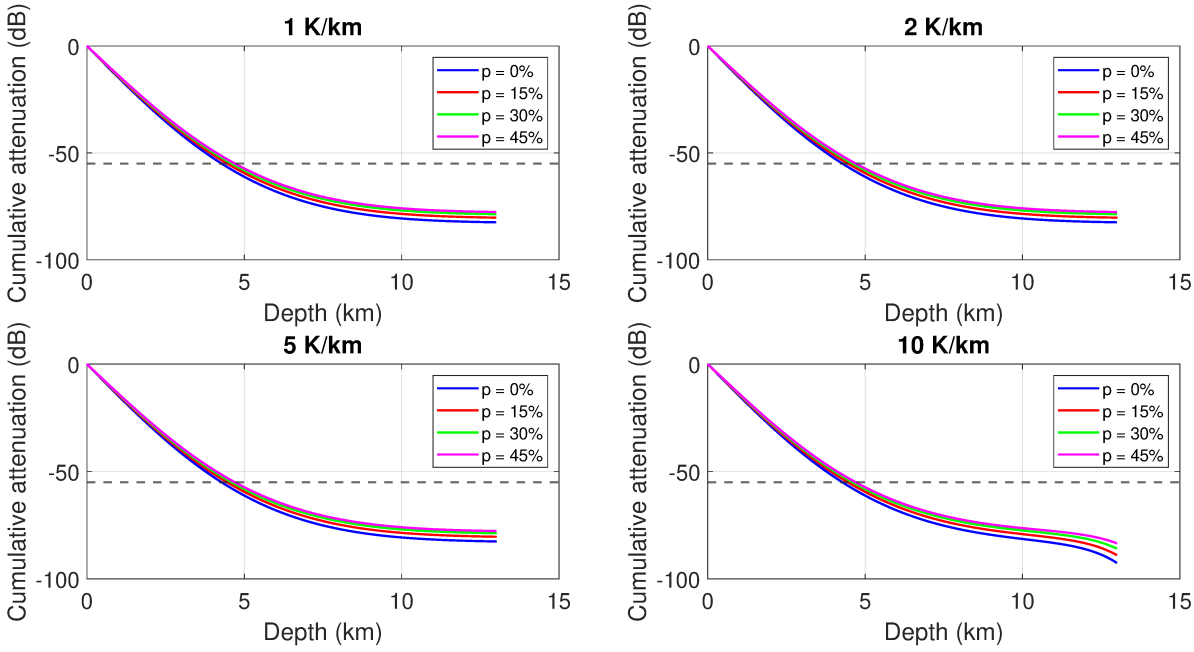

Figure 4.7: Cumulative attenuation in the case of Ganymede's bright terrains with the H5 meteoric contaminant.

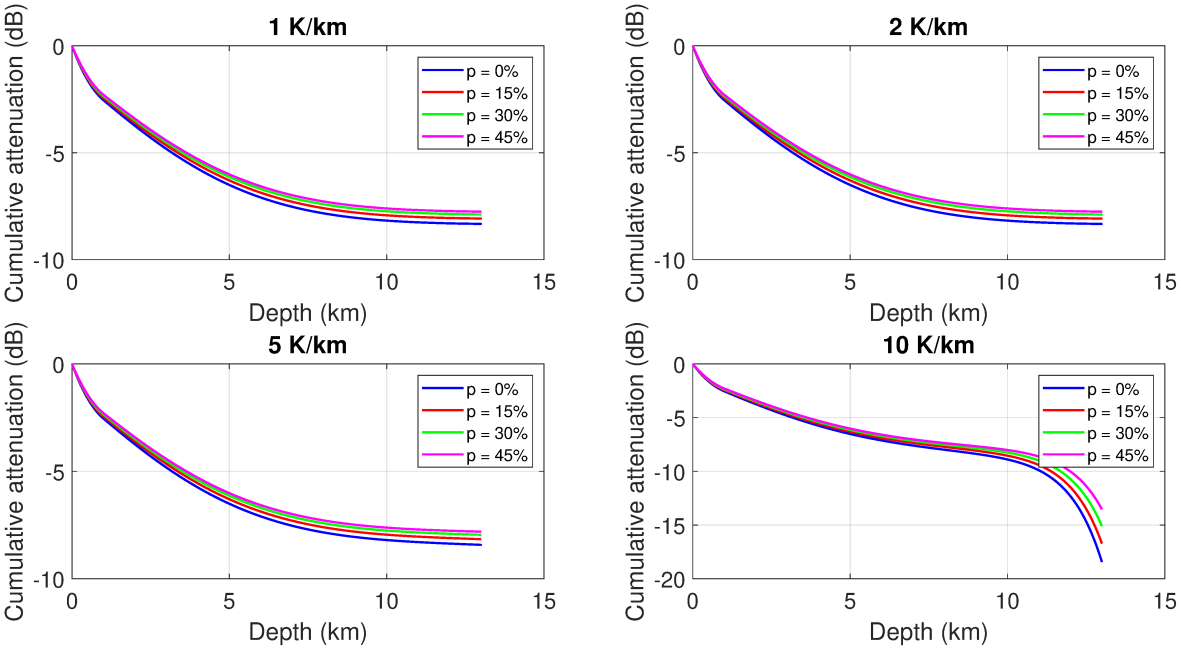

Figure 4.8: Cumulative attenuation in the case of Ganymede's dark terrains with the shergottite meteoric contaminant.

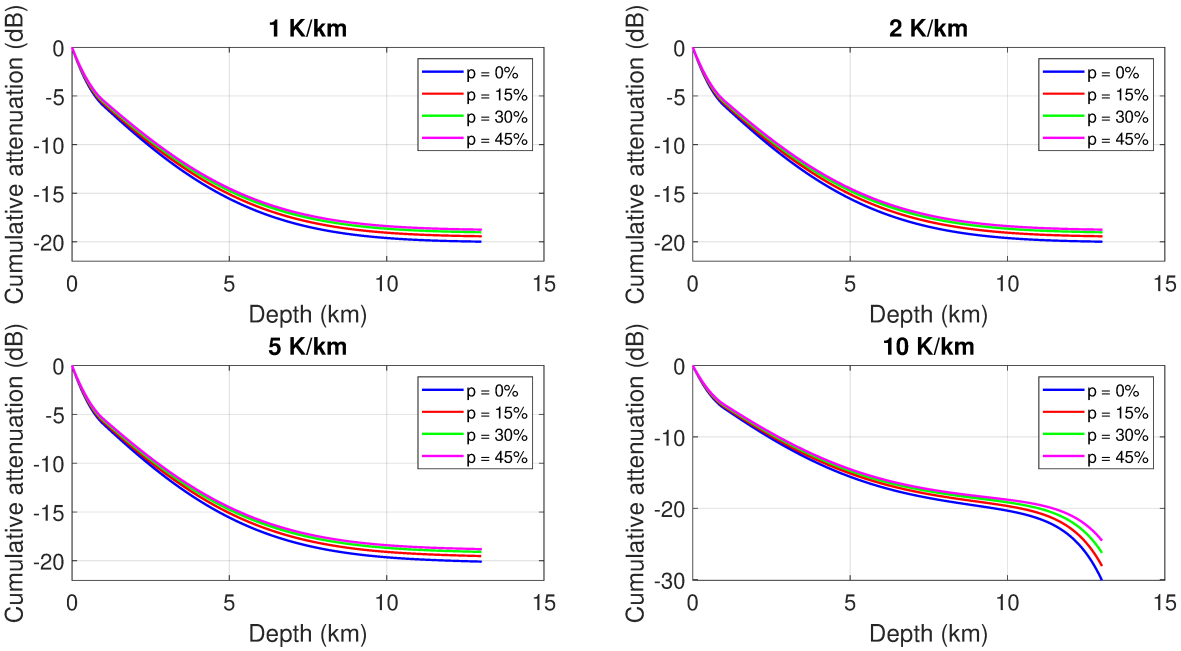

Figure 4.9: Cumulative attenuation in the case of Ganymede's dark terrains with the LL5 meteoric contaminant.

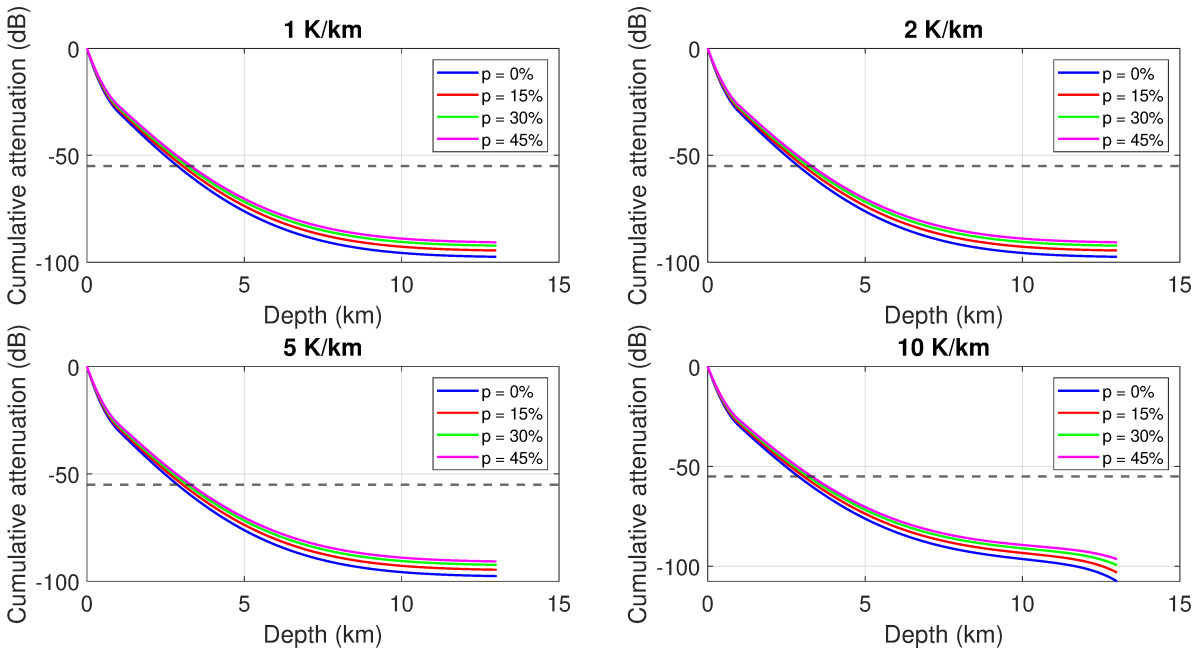

Figure 4.10: Cumulative attenuation in the case of Ganymede's dark terrains with the H5 meteoric contaminant.

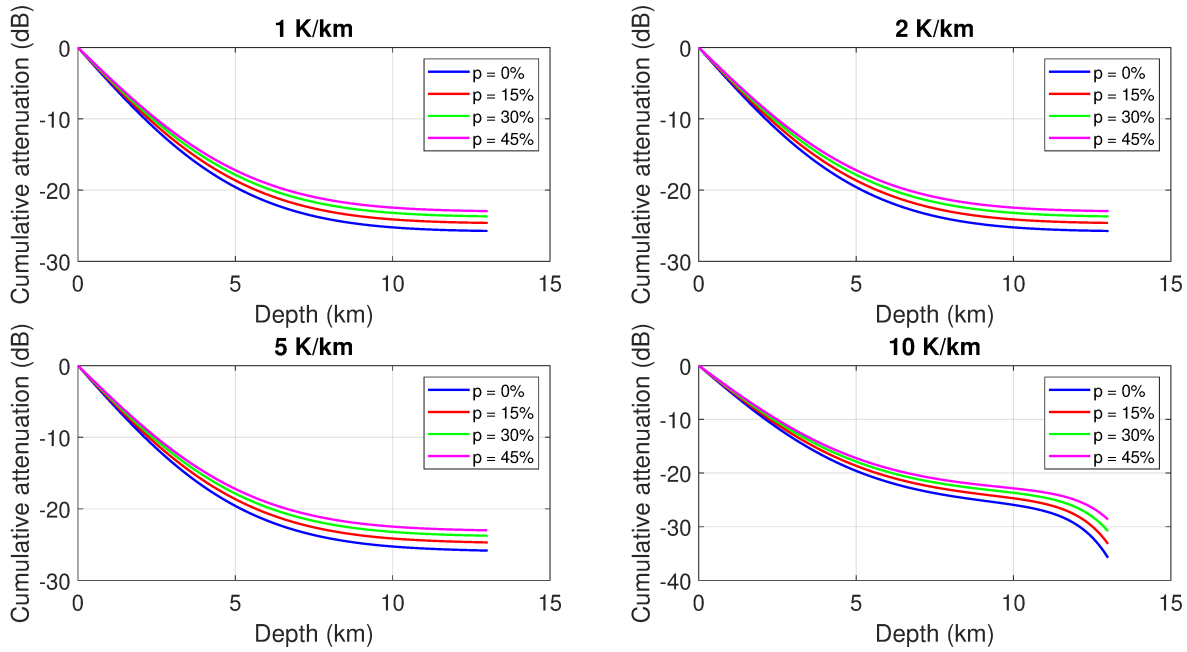

Figure 4.11: Cumulative attenuation in the case of Callisto (4.5 km standard deviation) with the shergottite meteoric contaminant.

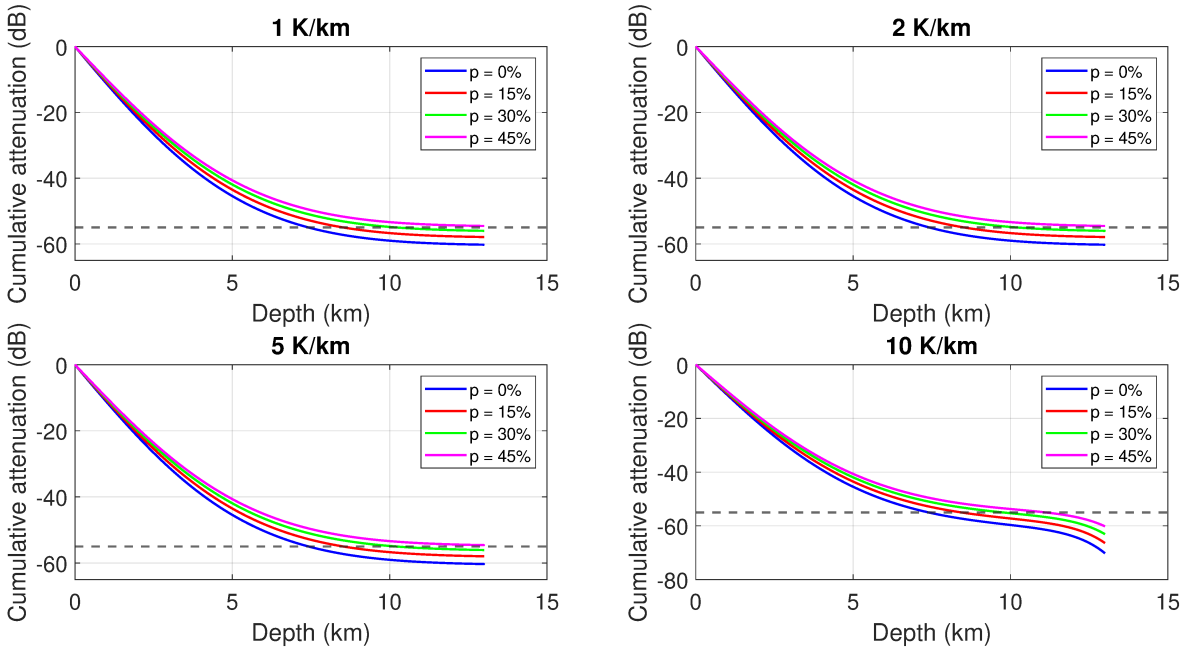

Figure 4.12: Cumulative attenuation in the case of Callisto (4.5 km standard deviation) with the LL5 meteoric contaminant.

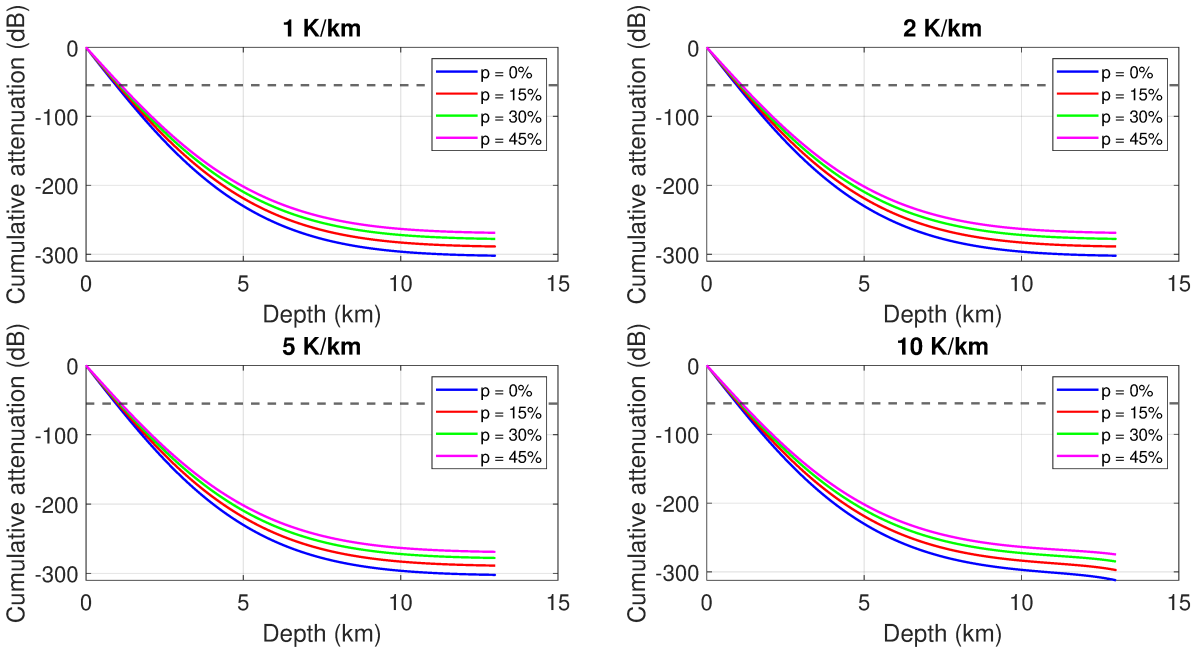

Figure 4.13: Cumulative attenuation in the case of Callisto (4.5 km standard deviation) with the H5 meteoric contaminant.

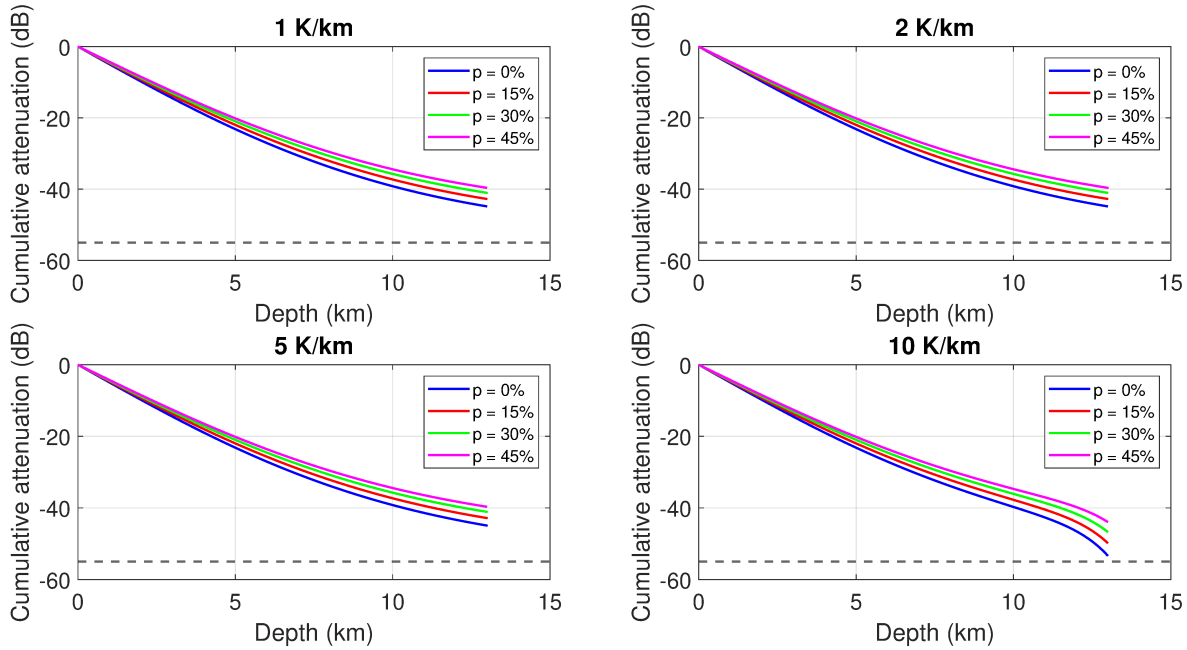

Figure 4.14: Cumulative attenuation in the case of Callisto (9 km standard deviation) with the shergottite contaminant.

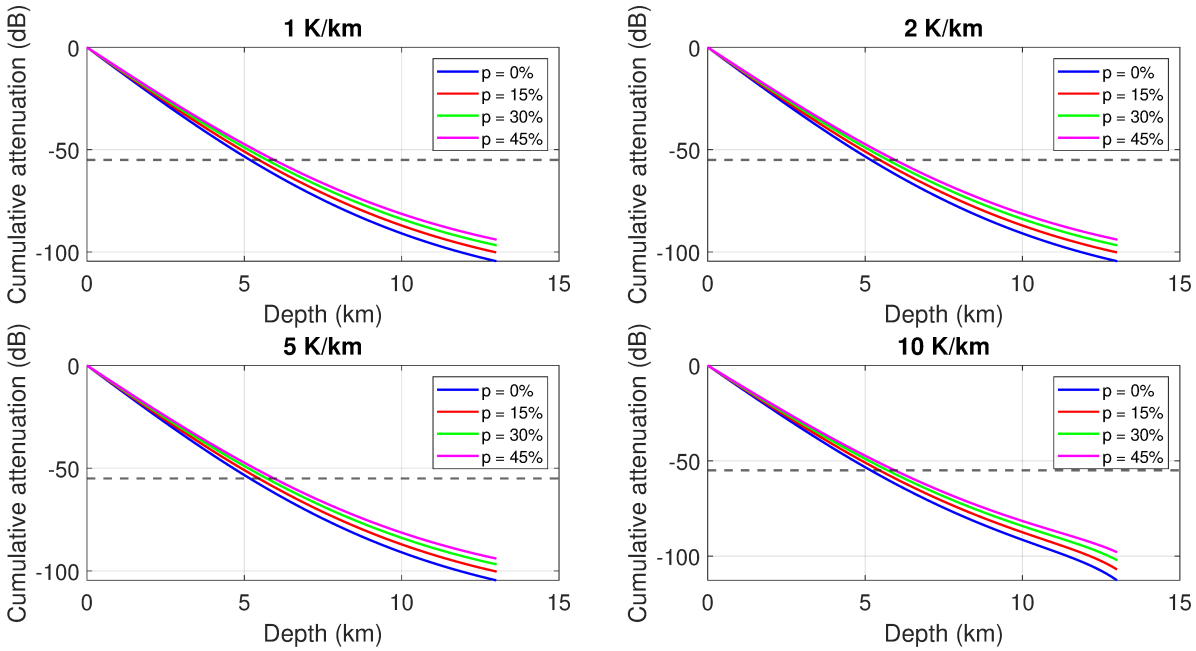

Figure 4.15: Cumulative attenuation in the case of Callisto (9 km standard deviation) with the LL5 meteoric contaminant.

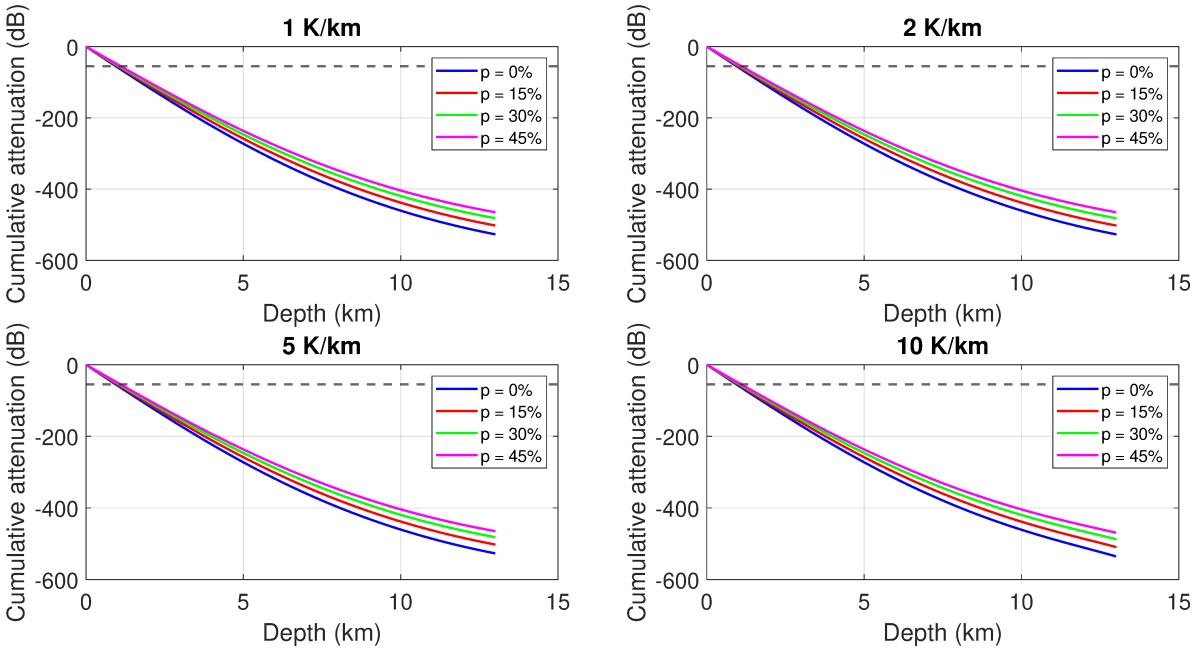

Figure 4.16: Cumulative attenuation in the case of Callisto (9 km standard deviation) with the H5 meteoric contaminant.

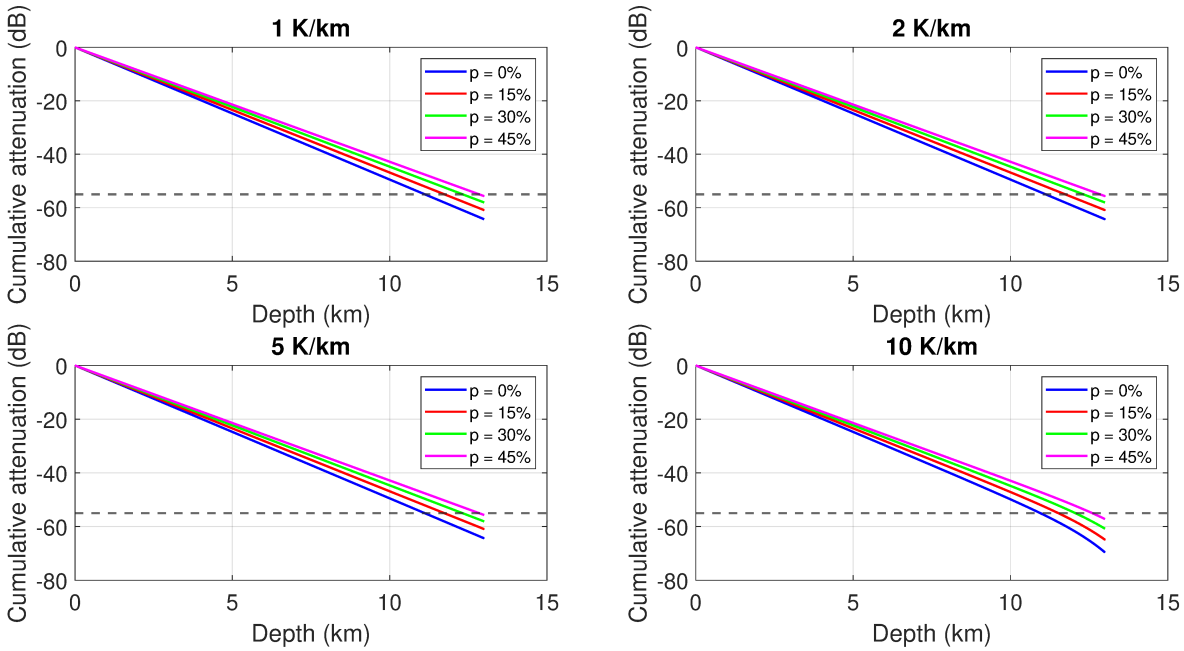

Figure 4.17: Cumulative attenuation in the case of Callisto (constant impurities) with the shergottite contaminant.

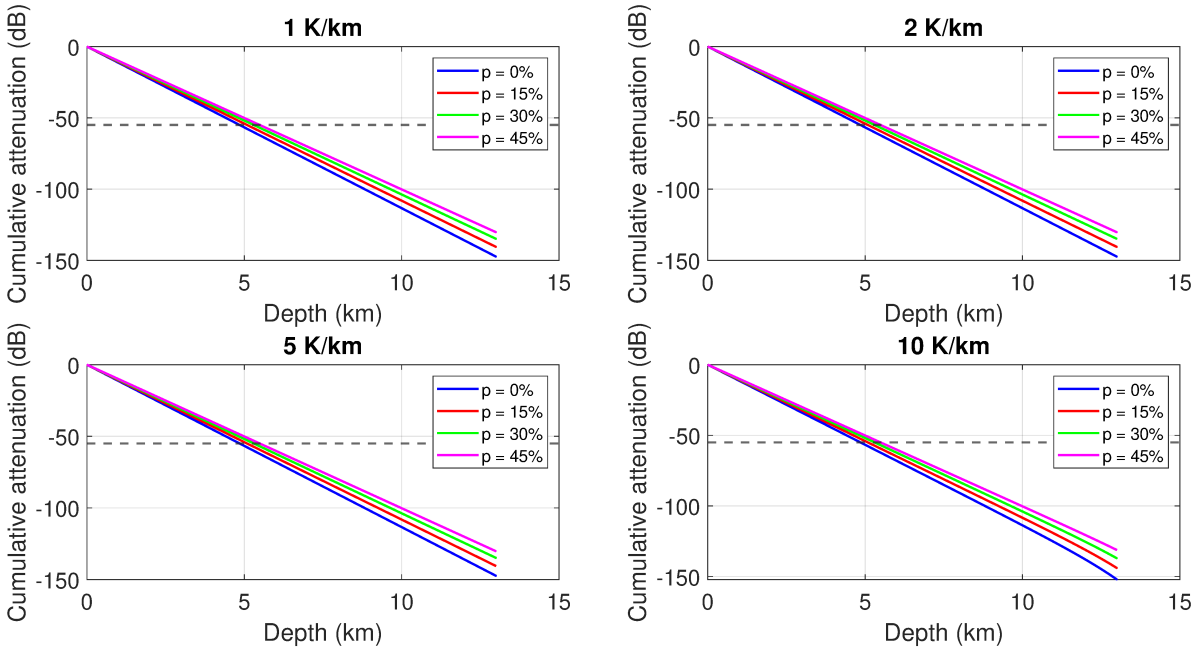

Figure 4.18: Cumulative attenuation in the case of Callisto (constant impurities) with the LL5 meteoric contaminant.

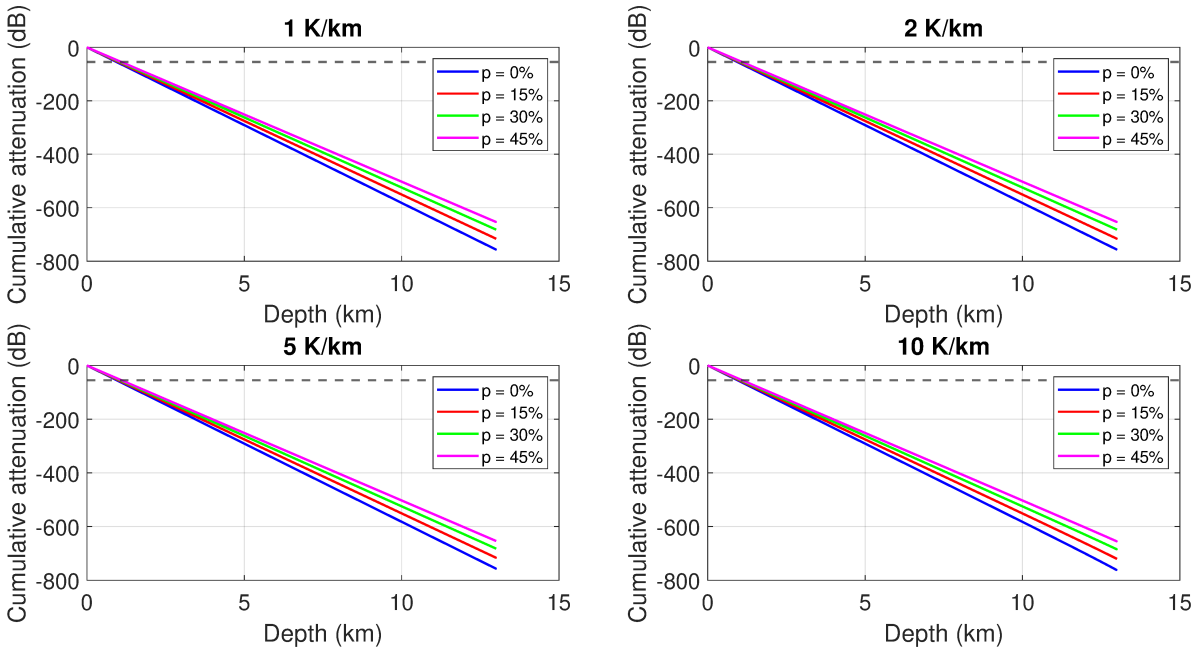

Figure 4.19: Cumulative attenuation in the case of Callisto (constant impurities) with the H5 meteoric contaminant.

4.3.2 Effect of temperature

In Section 4.2.1 have been discussed the values for the thermal gradients and the surface temperature. As said, the effect of temperature on the total cumulative attenuation is given by the increase of the imaginary permittivity of ice. In particular, Figure 4.1 shows that this component can have a significant effect only for temperatures greater than about 220 K. Given a surface temperature of 120 K, those values can be reached in the first 13 km only if the thermal gradient is very high, that is at least around 8 K/km. Such effect will therefore be stronger in the cases in which the ice abundance is higher, that is for Ganymede's bright terrains and zero porosity. The results for Ganymede's bright terrains are shown in Figures 4.5, 4.6, and 4.7. As shown, the curves are very similar for the first three thermal gradients, while the 10 K/km case shows a visible growth at depth. The imaginary permittivity of shergottite and amount of contaminant is so low (20% at the surface and decreasing downward), that ice attenuation dominates at depths greater than about 10 km in such case. In particular, attenuation is more or less doubled in the last 3 km. What's more, it can be observed that the cases with the LL5 and H5 contaminant show a smaller (in relative terms) increase, confirming that ice dominates attenuation when the abundance of impurities is low and the thermal gradient is large, unless the imaginary permittivity of the dust is high. In other words, the effect of temperature on ice (and therefore on the total cumulative attenuation) is strong if the permittivity of the contaminant is low and the thermal gradient is unrealistically high. As a contrast, it is interesting to look at the results obtained for the Callisto impurities profile with a 9 km standard deviation, shown in Figures 4.14, 4.15, and 4.16. This is the case with the highest amount of impurities (without considering the constant profile which, as already said, is unrealistic). In this case, the effect of temperature in the 10 K/km case is barely visible when considering the shergottite- or the LL5-like contaminant, and is not visible in the case with the H5 contaminant. This is explained by the fact that ice on Callisto does not dominate the chemical composition as it does in the case of Ganymede's bright terrains. It is possible to quantify the effect of temperature on ice by running the model using an impurity profile that is zero at all depths. The results are shown in figure 4.20. As can be appreciated, in the first three cases the total attenuation is always smaller than 10^{-1} dB, which explains why all the curves in the previous figures are extremely similar to one another, except when the thermal gradient is 10 K/km. In this last case, the cumulative attenuation ranges from about 6 to 10 dB, depending on the porosity. This is the difference between the first three and the last plot in each figure. As said, the effect is smaller in relative terms when the quantity of impurities and/or the imaginary permittivity of such are increased.

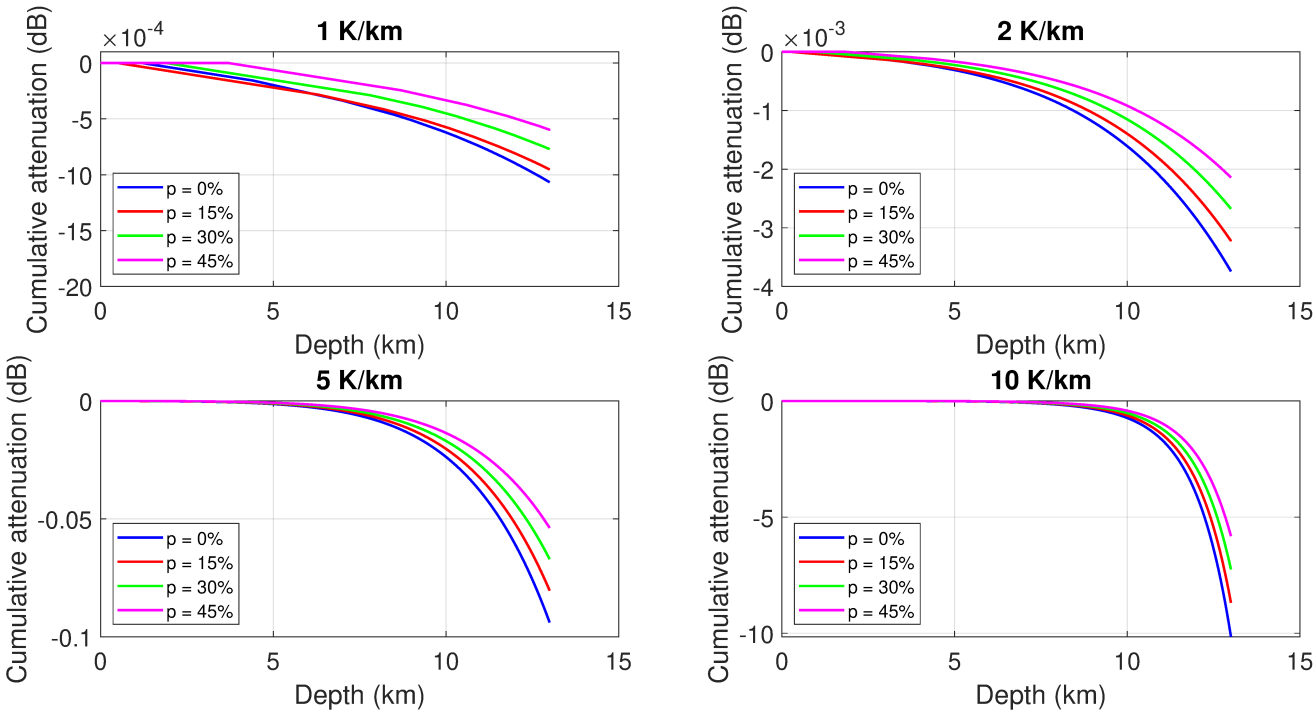

Figure 4.20: Cumulative attenuation in the absence of impurities.

4.3.3 Effect of porosity

As already mentioned, porosity is the least influential parameter affecting attenuation. Porosity introduces some parts that are made up of vacuum in the mixture and this lowers the effective permittivity since for vacuum $\varepsilon = 1 + 0i$ by definition. Therefore, fixed the other parameters, attenuation profiles with different porosities will have the same shape but with different absolute values. Let us consider Figure 4.6, which shows the results for the impurity profile of Ganymede's bright terrains and LL5 meteoric contaminant. Here, a very high porosity (45%) decreases the absolute value of the cumulative attenuation at 13 km by about 1 dB in the first three cases, which corresponds to a relative decrease of about 5%. However, in the last plot, the decrease caused by a 45% porosity is greater than 5 dB, corresponding to a relative decrease of about 19%. The explanation is quite simple: once the amount of dust is fixed, the rest of the composition is given by the sum of ice and vacuum. If the porosity is higher, naturally the amount of ice will be lower but, because of what is said in the previous section, ice strongly increases attenuation only at relatively high (> 220 K) temperatures. Therefore, the effect of porosity is stronger when the thermal gradient is large and allows ice to reach the temperature range in which its attenuation is strong.

When the thermal gradient is lower, the effect of ice on attenuation is barely noticeable, and therefore in such cases porosity has a smaller effect. Another fact can be noticed by comparing Figures 4.6 and 4.12. These correspond to two cases with the same contaminant but very different dust abundances (Ganymede's bright terrains and Callisto with a 4.5 km standard deviation, respectively). In the latter figure, in the first plot, the 45% porosity causes a relative decrease in attenuation of about 9%, much greater than the 5% found before for Ganymede's bright terrains. In the 10 K/km case, the decrease is about 10 dB, which corresponds to a relative decrease of about 14%. This means that when the thermal gradient is low since attenuation is dominated by the contaminant, porosity is relatively more effective when the amount of impurities is higher. On the other hand, a high thermal gradient significantly affects attenuation when the abundance of dust is small, as for Ganymede's bright terrains. Therefore, in the high-temperature gradient scenarios, porosity is relatively more effective when the impurity content is low. It is now possible to fix the impurity profile, for example, Ganymede's bright terrains, and to compare cases with different contaminants, such as the shergottite and the H5 chondrite. This is done by comparing Figures 4.5 and 4.7. In the former case, the relative decrease caused by a 45% porosity is nearly 6% for the 1 K/km case, while it is more than 27% for the 10 K/km case. For the H5 chondrite scenario, these values are nearly 6% and 10% respectively. This tells us that, when the thermal gradient is low, the effect of ice is negligible and therefore porosity has the same effect independently of the type of contaminant. When the thermal gradient is high enough to allow ice to have a significant effect, porosity is relatively less influential for a more attenuative contaminant (H5 chondrite), because this will largely dominate over ice. As a final remark, it is important to keep in mind that porosity is likely to be much smaller than the 45% discussed here, which is an extreme case. This allows once again to conclude that the effect of this quantity is to simply decrease attenuation by a factor that depends on the thermal gradient and the impurities content, but the influence that this parameter has is typically small compared to the influence of the thermal gradient (when high) and the impurities content themselves.

4.3.4 Effect of impurities

The effect of impurities can be described both in terms of abundance and of permittivity value. As obvious, the higher the contaminant abundance, the higher is the attenuation. The same for a contaminant with a higher imaginary permittivity. To better understand the effect of the different impurity profiles used, it is useful to look at Figure 4.21, which compares the attenuations obtained with different profiles but fixed contaminant, thermal gradient, and porosity. As expectable, all the curves tend to become flat at depth, because of the gaussian decreasing amount of impurities. On

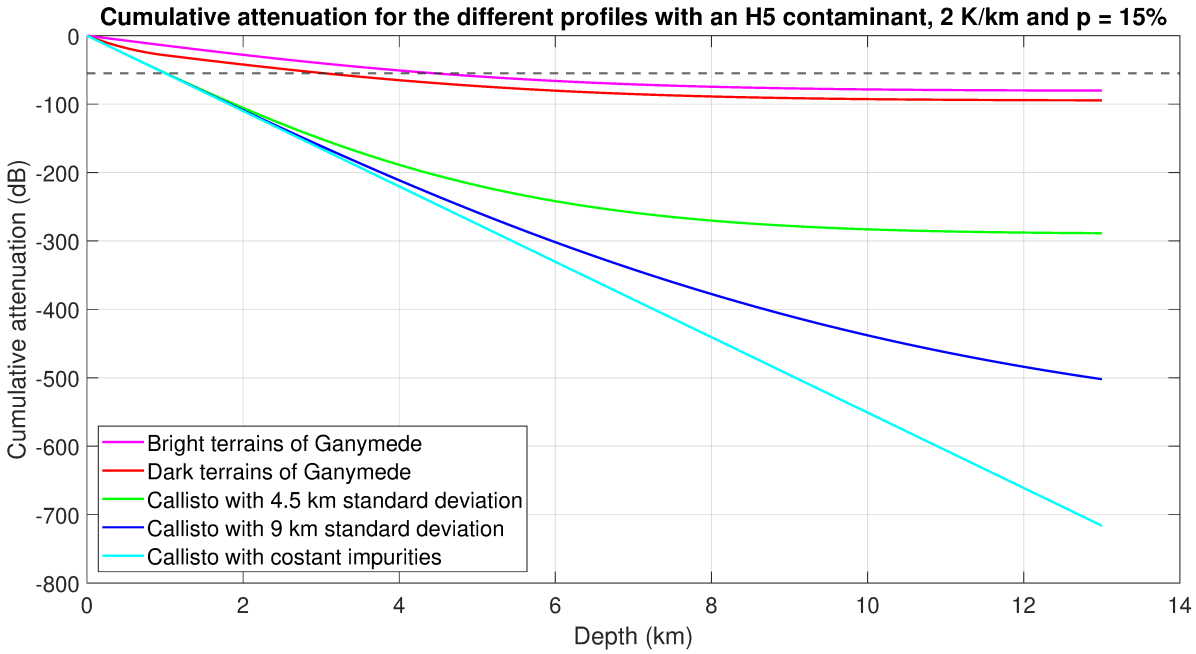

Figure 4.21: Cumulative attenuation for the different impurity profiles with an H5 contaminant, a thermal gradient of 2 K/km, and a 15% porosity.

the contrary, the constant-impurity profile causes attenuation to linearly ($R^2 = 1$) increase with depth. This figure confirms that the difference between Ganymede's bright and dark terrains is rather small if compared to the different cases treated for Callisto. Among these, the differences are far greater, because of the strongly increasing overall presence of contaminants. Looking at the two Ganymede's profiles, it can be seen that the dark terrains reach an attenuation that is 15% higher than that of the bright terrains. Such difference is given only by the impurity-rich layer at the top which, in these simulations, is only 1 km thick. If such a layer were thicker, it could cause an even greater difference, so that the dark areas of Ganymede will be much more difficult to probe than the bright areas. The situation on Callisto is even worse, because of the much higher dust abundance. As shown, Callisto has been assumed to have a surface impurity content that is more than 3 times higher than that of Ganymede's bright terrains, and this is translated into an attenuation that is more than 3 times higher. On Callisto, doubling the standard deviation of the impurity profile leads to an increase in the total attenuation of 74%.
As already explained, the key factor in determining the radar attenuation is the imaginary permittivity of the medium. If the thermal gradient is low, as explained, this is dominated by the value of the non-ice component. Porosity can also decrease the resulting permittivity if it is high, as described in

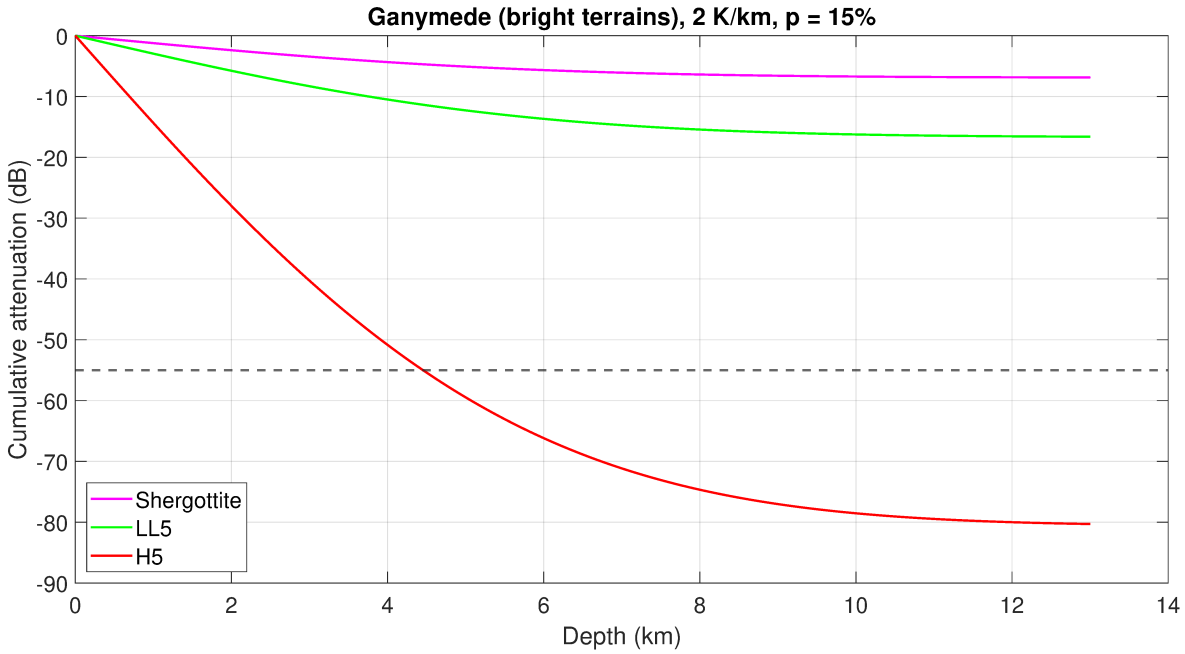

Figure 4.22: Cumulative attenuation for the three different contaminants for Ganymede's bright terrains, a thermal gradient of 2 K/km, and a 15% porosity.

Section 4.3.3. The imaginary permittivity of the LL5 contaminant is nearly twice that of shergottite, and that of the H5 contaminant is more than 6 times that of the LL5 (so almost 12 times that of shergottite). It is possible to compare the different attenuations that these contaminants cause, for example, in Figure 4.22. This shows the results for Ganymede's bright terrain and the different types of impurities, with fixed porosity and thermal gradient. The attenuation for the LL5 case is more than twice that of shergottite, while in the H5 case it is almost 12 times that of shergottite. The same holds for the other profiles. This means that, although attenuation increases linearly with the imaginary permittivity for pure water ice (equation 1.8), this is not true for the effective permittivity that results from the mixing formula. Otherwise, the attenuation obtained in the LL5 cases would be almost twice that obtained in the shergottite cases (instead, the ratio is about 2.5). In any case, Figures 4.22 shows the great influence that the type of contaminant can have. In the case of Ganymede's bright terrains, a more or less attenuative impurity can make a huge difference in the depth that can be reached.

4.4 Observational perspective

4.4.1 Detectability limits

Now that the different scenarios have been explored, it is important to determine what RIME could be able to detect. As shown in the previous sections, at Ganymede's bright terrains the amount of impurities is so low that, in most scenarios, the attenuation is abundantly below the observational limit. Water ice is almost pure here and allows a great radar penetration. The results obtained for Ganymede's bright terrains demonstrate that RIME will presumably be able to probe a great depth if the contaminant is similar to the shergottite or the LL5 sample used here. On the other hand, if the contaminant is more like the H5 used here, it will not be possible to reach depths greater than about 4 or 5 km (and even an extremely high porosity does not better the situation). The situation is not so different for the dark terrains, where the top impurity-rich layer is not enough to greatly enhance the total attenuation. However, even if the situation were similar to the H5 scenario simulated here, it would not be so bad: a depth of 5 km should still be enough to detect a series of geological features that are expected to be present right under Ganymede's surface (e.g., Heggy et al. (2017); Bjonnes et al. (2018)), reaching the scientific goals of the mission (Bruzzone et al., 2015). In the case of Callisto with a 4.5 km standard deviation, the situation strongly depends on the actual contaminant. If this is similar to a shergottite, then the attenuation remains below the detectability limit even in the worst case with zero porosity and a thermal gradient of 10 K/km. In the LL5 contaminant scenario, the depth at which the 55 dB observational limit is reached is greatly affected by porosity, as visible in Figure 4.12. For zero porosity, it could be possible to investigate only the first 7 km, while for a very high porosity it could be possible to reach a depth of 10 km. For a more attenuative contaminant like the H5 type, the expected detectability limit should be reached in the first 2 km, and this would cause a very poor scientific return. Even in the case in which the impurity profile has a 9 km standard deviation, with a low-permittivity contaminant like the shergottite, it would still be possible to reach a depth of at least 13 km. As explained, this scenario is not so unrealistic, considering the lack of differentiation that is likely for Callisto. The case with the LL5 contaminant is made significantly worse, since in this situation the reachable depth is around 5 or 6 km, depending on the porosity. When the assumed contaminant is the H5, the 55 dB limit is reached in the first 2 km, similar to the previous case. This happens because the two impurity profiles are similar close to the surface even if the two standard deviations are different. At last, let us consider the unrealistic scenario in which the amount of impurity remains constant with depth. If the contaminant is similar to the shergottite, even in such an extreme case, a depth of about 11 or12 km (depending on porosity) can

presumably be reached. With an LL5 contaminant, the situation is similar to the previous case, and RIME could see up to a depth of about 5 km. Once again, with an H5 contaminant, the penetration depth is not greater than about 2 km.

4.4.2 Most realistic scenarios

In the previous section, all the different scenarios explored with this model have been described. However, as previously mentioned, not all these scenarios are equally likely to be representative of the situation on Ganymede or Callisto. As described in Section 4.2.1, the temperature gradient is more likely to be smaller than 5 K/km. Because of the temperature dependence of the imaginary permittivity of ice, using a thermal gradient of 1 or 2 K/km yields basically to the same result. Here, the most realistic case considered is the one with 2 K/km, in analogy to Heggy et al. (2017). As far as the porosity is concerned, the 45% value used here as an upper limit likely represents an overestimate of such parameter. I would tend to consider $p = 0\%$ as the most realistic value, assuming that a non-zero porosity that might be present at the surface is likely to rapidly decrease with depth. However, it is better to be cautious, since the assumption of a rapid drop of porosity is based on the behavior of Earth rocks, which have a different chemical composition from the ones likely to be present on the icy satellites. What's more, the surface gravity of these bodies is much lower than that of Earth. Therefore, I will assume a porosity of 15% to be the most representative of these bodies. Again, this is similar to what was done by Heggy et al. (2017), who assumed a constant 10% porosity. Unfortunately, there are today no constrains on the possible impurity profiles inside planetary bodies. The gaussian behavior assumed here is purely arbitrary and could even be unrealistic. The only realistic assumptions regard the surface values for the impurity content. A point difficult to parametrize is the impurity-rich layer assumed for Ganymede's dark terrains. Here, it has been assumed to be linear to make it rather different from the otherwise Gaussian profile. This is an important problem that RIME will hopefully help to solve. For Callisto, I believe that the profile with a 9 km standard deviation is the most realistic among the ones considered because the constant profile could be likely for a completely undifferentiated body, while Callisto should have at least some degree of differentiation. On the other hand, it is less differentiated than Ganymede, therefore a higher standard deviation for the impurity profile is more likely (although it might have a very different value from the 9 km used here). As far as the type of contaminant is concerned, it is now impossible to say which one is the most realistic. What's more, if it is true that the contaminant is of meteoric type, several other possibilities have not been explored here. The only thing that can be said is that, hopefully, the contaminant has a low imaginary permittivity like the shergottite analog

used here. However, if it is similar to the H5 sample used here, the situation will be far more dramatic.
With all this in mind, what can be concluded about the future RIME observations? If the model used here is realistic, and if the values for the parameters discussed above are indeed representative of the situation on Ganymede and Callisto, then on Ganymede RIME could be able to penetrate even more than 13 km into the crust, both below the bright and the dark terrains, with a favorable contaminant. The same holds for Callisto if the contaminant is similar to the shergottite analog used here, but if it is more similar to the H5 analog then the radar will not penetrate over the first 2 km. This would be an extremely bad situation since it probably would not allow the detection of any interesting feature. The resulting penetration depths (expressed in kilometers) accounting for the 55 dB observational limit are shown in Table 4.2 for all the different contaminants and impurity profiles explored. The reported results refer to the most realistic scenario with a thermal gradient of 2 K/km and a 15% porosity.

Impurity profile	Shergottite	LL5 chondrite	H5 chondrite
Ganymede's brigh terrains	> 13	> 13	4.45
Ganymede's dark terrains	> 13	> 13	3.04
Callisto (4.5 km standard deviation)	> 13	8.53	1.01
Callisto (9 km standard deviation)	> 13	5.46	1.00
Callisto (constant impurities)	11.74	5.09	1.00

Table 4.2: Penetration depths (in kilometers) for different impurity profiles and contaminants, assuming a 2 K/km thermal gradient and a 15% porosity.

4.5 Limits of the model

As a final remark, it is important to consider that the model used here has different limitations. These are mainly due to factors that have been

neglected, but that may play an important role in determining the radar attenuation on Ganymede and Callisto. RIME will eventually have to do with such factors. The first element neglected here is the presence of geological structures. This has been done, for example, by Heggy et al. (2017). However, they fixed the other parameters such as the thermal gradient, the porosity, the impurity profiles, and the impurities permittivities. In a way, it could be said that this work and their work are complementary. In the case of Callisto, the only relevant geological structure that they propose are knobs, which are what remains of ancient crater rims. They also state that the rough surface can give rise to a strong surface clutter that here has not been considered. On the other hand, Ganymede has more complicated and evident structures, and probably several cracks under the surface. The furrow systems on Ganymede's dark terrains should cause a strong surface clutter, while the several cracks under the bright terrains should cause volume scattering, another effect that has here been neglected. Another work whose aim is to estimate volume scattering for the Galilean satellites is the one by Di Paolo et al. (2018). The authors concluded that volume scattering by spherical voids should not be significant for Ganymede and Callisto. Another way in which this work is limited regards the impurity profiles and the contaminant used. Although different profiles have been used, it could be possible to explore, for example, power-law impurity profiles. What's more, here only three different contaminants have been used. A way to expand this work would consist of using other meteoric-like contaminants over a wider range of permittivities. Also, it could be possible to mix more types of impurities when evaluating the effective permittivity through the Rayleigh mixing formula.

Chapter 5

Conclusions

As described in Chapter 1, Ganymede and Callisto are two extremely interesting satellites that need to be studied more since there are still several unresolved problems. One way in which this can be done is through radar sounding, a technique thanks to which interesting results have already been obtained for Mars using the MARSIS and SHARAD instruments. The fact that the outer satellites of our Solar System are mainly made up of water ice allows the use of such an effective technique. However, the effect of temperature, porosity, and presence of non-water materials makes the situation not so easy to study. In Chapter 4, the effects of all these parameters have been discussed, showing that different scenarios can make the work of RIME very easy or very challenging: the penetration depth can vary from 1 to far more than 13 km, depending on the type and amount of impurities.
In a few years, the data from this mission will surely help to place better constraints than the ones we have today on a series of features of these two satellites. It will be possible to detect the geological elements that are supposed to be present below the surface and that are, today, unobservable. The presence of these elements will help to understand the geology of these worlds and their putative past activity. This, in turn, will also give helpful information about the orbital evolution of Ganymede and Callisto, and the Laplace resonance. A better constrain of the thermal gradient will allow us to determine the amount of heat stored in the interior, and maybe a better estimate of the depth at which the subsurface salty ocean must lay. Probably, the most important result that we can hope to obtain in this way is a precise determination of the type of non-water constituents present in these bodies. This is very important since it can be linked to the theoretical formation models.
Since RIME will not be at work for twelve more years, there is still so much work than can be done to obtain better dielectric models and, therefore, more reliable values for the cumulative attenuation and penetration depth. It is possible to use theoretical models to determine more precisely what

the thermal gradient could be. It is possible to carry out experiments to measure how the porosity may vary inside bodies that are so different from our planet. Another improvement can come from more dielectric measurements of a wider range of possible contaminants that might be present in the outer regions of the Solar System. Finally, a model accounting for both the presence of geological structures and a wide space of variables (temperature profile, porosity, impurity gradient, and impurity permittivity) will allow us to construct the most realistic scenario possible.

Ringraziamenti

Vorrei ringraziare il dottor Claudi per avermi inizialmente fatto una proposta di tesi che riguardasse questo ambito, e che mi ha portato a svolgere questo lavoro. Vorrei ringraziare tutto il team dell'università di Roma Tre per l'aiuto, soprattutto Federico che ha dedicato più tempo di chiunque altro a supervisionarmi nella stesura della tesi. Vorrei infine ringraziare la mia ragazza per l'immancabile e incondizionato supporto morale durante tutto il tempo che mi è stato necessario per completare questo lavoro.

Bibliography

Baron, J. E., Tyler, G. L., and Simpson, R. A. (2003). Three-dimensional numerical modeling of refraction and reflection scattering from icy galilean satellites. *Icarus*, 164(2):404–417.

Bjonnes, E. E., Johnson, B. C., and Silber, E. A. (2018). Formation of Impact Craters on Ganymede and Callisto as a Constraint on Ice Shell Structure. In *Lunar and Planetary Science Conference*, Lunar and Planetary Science Conference, page 1548.

Black, G. J., Campbell, D. B., and Nicholson, P. D. (2001). Icy Galilean Satellites: Modeling Radar Reflectivities as a Coherent Backscatter Effect. *Icarus*, 151(2):167–180.

Blankenship, D. D., Young, D. A., Moore, W. B., and Moore, J. C. (2009). Radar Sounding of Europa's Subsurface Properties and Processes: The View from Earth. In *European Planetary Science Congress 2009*, page 636.

Brouet, Y., Neves, L., Sabouroux, P., Levasseur-Regourd, A. C., Poch, O., Encrenaz, P., Pommerol, A., Thomas, N., and Kofman, W. (2016). Characterization of the permittivity of controlled porous water ice-dust mixtures to support the radar exploration of icy bodies. *Journal of Geophysical Research (Planets)*, 121(12):2426–2443.

Bruzzone, L., Plaut, J., Alberti, G., Blankenship, D., Bovolo, F., Campbell, B., Castelletti, D., Gim, Y., Ilisei, A.-M., Kofman, W., Komatsu, G., Mckinnon, W., Mitri, G., Moussessian, A., Notarnicola, C., Orosei, R., Patterson, G., Pettinelli, E., and Plettemeier, D. (2015). Jupiter icy moon explorer (juice): Advances in the design of the radar for icy moons (rime). *IGARSS 2015 - 2015 IEEE International Geoscience and Remote Sensing Symposium*, pages 1257–1260.

Bruzzone, L., Plaut, J. J., Alberti, G., Blankenship, D. D., Bovolo, F., Campbell, B. A., Ferro, A., Gim, Y., Kofman, W., Komatsu, G., McKinnon, W., Mitri, G., Orosei, R., Patterson, G. W., Plettemeier, D., and Seu, R. (2013). RIME: Radar for Icy Moon Exploration. In *European Planetary Science Congress*, pages EPSC2013–744.

Byrne, P. K., Regensburger, P. V., Klimczak, C., Bohnenstiehl, D. R., Hauck, S. A., Dombard, A. J., and Hemingway, D. J. (2018). The Geology of the Rocky Interiors of Enceladus, Europa, Titan, and Ganymede. In *Ocean Worlds*, volume 2085, page 6030.

Calvin, W. M. and Clark, R. N. (1991). Modeling the reflectance spectrum of Callisto 0.25 to 4.1 μm. *Icarus*, 89(2):305–317.

Calvin, W. M. and Clark, R. N. (1993). Spectral Distinctions between the Leading and Trailing Hemispheres of Callisto: New Observations. *Icarus*, 104(1):69–78.

Calvin, W. M., Clark, R. N., Brown, R. H., and Spencer, J. R. (1995). Spectra of the icy Galilean satellites from 0.2 to 5 μm: A compilation, new observations, and a recent summary. *Journal of Geophysical Research*, 100(E9):19041–19048.

Chyba, C. F., Ostro, S. J., and Edwards, B. C. (1998). Radar Detectability of a Subsurface Ocean on Europa. *Icarus*, 134(2):292–302.

Clark, R. N. (1980). Ganymede, Europa, Callisto, and Saturn's rings: Compositional analysis from reflectance spectroscopy. *Icarus*, 44(2):388–409.

Clark, R. N., Fanale, F. P., and Gaffey, M. J. (1986). Surface composition of natural satellites. In *Satellites*, pages 437–491.

Consolmagno, G. J. and Lewis, J. S. (1976). Structural and thermal models of icy Galilean satellites. In Gehrels, T. and Matthews, S., editors, *IAU Colloq. 30: Jupiter: Studies of the Interior, Atmosp here, Magnetosphere and Satellites*, pages 1035–1051.

Consolmagno, G. J. and Lewis, J. S. (1977). Preliminary thermal history models of icy satellites. In *IAU Colloq. 28: Planetary Satellites*, pages 492–500.

Croft, S. K. (1993). Porosity and the Ecology of Icy Satellites. In *Lunar and Planetary Science Conference*, Lunar and Planetary Science Conference, page 347.

Dalton, J. B. (2010). Spectroscopy of Icy Moon Surface Materials. *Space Science Reviews*, 153(1-4):219–247.

Dalton, J. B., Cruikshank, D. P., Stephan, K., McCord, T. B., Coustenis, A., Carlson, R. W., and Coradini, A. (2010). Chemical Composition of Icy Satellite Surfaces. *Space Science Reviews*, 153(1-4):113–154.

Das, T. and Mukherjee, S. (2020). *Compaction of Sediments and Different Compaction Models*, pages 1–8.

Di Paolo, F., Orosei, R., Lauro, S., Cosciotti, B., Mattei, E., and Pettinelli, E. (2018). Volume scattering losses evaluation for radar sounding of jovian icy moons. pages 2422–2425.

Eluszkiewicz, J. and Leliwa-Kopystynski, J. (1988). A model of the porous structure of icy satellites. *Lunar and Planetary Science Conference Proceedings*, 18:741–747.

Grasset, O., Dougherty, M. K., Coustenis, A., Bunce, E. J., Erd, C., Titov, D., Blanc, M., Coates, A., Drossart, P., Fletcher, L. N., Hussmann, H., Jaumann, R., Krupp, N., Lebreton, J. P., Prieto-Ballesteros, O., Tortora, P., Tosi, F., and Van Hoolst, T. (2013). JUpiter ICy moons Explorer (JUICE): An ESA mission to orbit Ganymede and to characterise the Jupiter system. *Planetary and Space Science*, 78:1–21.

Hammond, N. P. and Barr, A. C. (2013). Determining Ice Shell Conditions Conducive to Convection-Driven Grooved Terrain Formation on Ganymede. In *Lunar and Planetary Science Conference*, Lunar and Planetary Science Conference, page 1771.

Heggy, E., Palmer, E. M., Kofman, W., Clifford, S. M., Righter, K., and Hérique, A. (2012). Radar properties of comets: Parametric dielectric modeling of Comet 67P/Churyumov-Gerasimenko. *Icarus*, 221(2):925–939.

Heggy, E., Scabbia, G., Bruzzone, L., and Pappalardo, R. T. (2017). Radar probing of Jovian icy moons: Understanding subsurface water and structure detectability in the JUICE and Europa missions. *Icarus*, 285:237–251.

Helfenstein, P., Veverka, J., Denk, T., Neukum, G., Head, J. W., Pappalardo, R., and Galileo IMAGING Team (1997). Dark-Floor Craters: Galileo Constraints on a Ganymede Regolith Component. In *Lunar and Planetary Science Conference*, Lunar and Planetary Science Conference, page 547.

Herique, A., Agnus, B., Asphaug, E., Barucci, A., Beck, P., Bellerose, J., Biele, J., Bonal, L., Bousquet, P., Bruzzone, L., Buck, C., Carnelli, I., Cheng, A., Ciarletti, V., Delbo, M., Du, J., Du, X., Eyraud, C., Fa, W., Gil Fernandez, J., Gassot, O., Granados-Alfaro, R., Green, S. F., Grieger, B., Grundmann, J. T., Grygorczuk, J., Hahnel, R., Heggy, E., Ho, T. M., Karatekin, O., Kasaba, Y., Kobayashi, T., Kofman, W., Krause, C., Kumamoto, A., Küppers, M., Laabs, M., Lange, C., Lasue, J., Levasseur-Regourd, A. C., Mallet, A., Michel, P., Mottola, S., Murdoch, N., Mütze, M., Oberst, J., Orosei, R., Plettemeier, D., Rochat, S., RodriguezSuquet, R., Rogez, Y., Schaffer, P., Snodgrass, C., Souyris, J. C., Tokarz, M., Ulamec, S., Wahlund, J. E., and Zine, S. (2018). Direct observations of asteroid interior and regolith structure: Science measurement requirements. *Advances in Space Research*, 62(8):2141–2162.

Kargel, J. S. (1991). Brine volcanism and the interior structures of asteroids and icy satellites. *Icarus*, 94(2):368–390.

Kawada, S. (1978). Dielectric anisotropy in ice ih. *Journal of the Physical Society of Japan*, 44(6):1881–1886.

Kimura, J. and Kuramoto, K. (2010). Internal differentiation and thermal history of giant icy moons: implications for the dichotomy between Ganymede and Callisto. In *European Planetary Science Congress 2010*.

Kimura, J. and Kuramoto, K. (2011). Turning point in differentiation history between Ganymede and Callisto induced by dehydration of primitive hydrous rock. In *EPSC-DPS Joint Meeting 2011*, volume 2011, page 358.

Kimura, J., Nakagawa, T., and Kurita, K. (2009). Size and compositional constraints of Ganymede's metallic core for driving an active dynamo. *Icarus*, 202(1):216–224.

Kofman, W. and Safaeinili, A. (2004). Radar Techniques Applied to Subsurface Studies in Solar System Exploration. In Battrick, B., editor, *Tools and Technologies for Future Planetary Exploration*, volume 543 of *ESA Special Publication*, pages 39–50.

Kuskov, O. L. and Kronrod, V. A. (2005). Internal structure of Europa and Callisto. *Icarus*, 177(2):550–569.

Lewis, J. S. (1971). Satellites of the Outer Planets: Their Physical and Chemical Nature. *Icarus*, 15(2):174–185.

Ligier, N., Calvin, W. M., Carter, J., Paranicas, C., Poulet, F., and Snodgrass, C. (2019a). New insights about Callisto's surface composition and properties from ground-based observations. In *EPSC-DPS Joint Meeting 2019*, volume 2019, pages EPSC–DPS2019–491.

Ligier, N., Calvin, W. M., Carter, J., Poulet, F., Paranicas, C., and Snodgrass, C. (2020). New Insights into Callisto's Surface Composition with the Ground-Based Near-Infrared Imaging Spectrometer SINFONI of the VLT. In *Lunar and Planetary Science Conference*, Lunar and Planetary Science Conference, page 1959.

Ligier, N., Paranicas, C., Carter, J., Poulet, F., Calvin, W. M., Nordheim, T. A., Snodgrass, C., and Férellec, L. (2019b). Properties and Composition of Ganymede's Surface: Updates from Near-Infrared Ground-Based Observations with SINFONI/VLT/ESO. In *Lunar and Planetary Science Conference*, Lunar and Planetary Science Conference, page 1214.

Ligier, N., Paranicas, C., Carter, J., Poulet, F., Calvin, W. M., Nordheim, T. A., Snodgrass, C., and Ferellec, L. (2019c). Surface composition and properties of Ganymede: Updates from ground-based observations with the near-infrared imaging spectrometer SINFONI/VLT/ESO. *Icarus*, 333:496–515.

Lucchetti, A., Pozzobon, R., Pajola, M., Mazzarini, F., Cremonese, G., and Massironi, M. (2020). Fractal Analysis on Ganymede Grooves: Insights into the Icy Shell Thickness of the Satellite. In *Lunar and Planetary Science Conference*, Lunar and Planetary Science Conference, page 1401.

McKinnon, W. B. (2004). Overview of Europa's Icy Shell: Questions of Thickness, Composition, Rheology, Tectonics, and Astrobiological Potential. In Schenk, P., Nimmo, F., and Prockter, L., editors, *Workshop on Europa's Icy Shell: Past, Present, and Future*, page 7048.

McKinnon, W. B. (2005). Radar Sounding of Convecting Ice Shells in the Presence of Convection: Application to Europa, Ganymede, and Callisto. In *Workshop on Radar Investigations of Planetary and Terrestrial Environments*, page 53.

McKinnon, W. B. (2006). On convection in ice I shells of outer Solar System bodies, with detailed application to Callisto. *Icarus*, 183(2):435–450.

McKinnon, W. B. and Parmentier, E. M. (1986). *Ganymede and Callisto*, pages 718–763.

Monteux, J., Golabek, G. J., Rubie, D. C., Tobie, G., and Young, E. D. (2018). Water and the Interior Structure of Terrestrial Planets and Icy Bodies. *Space Science Reviews*, 214(1):39.

Moore, J. M., Chapman, C. R., Bierhaus, E. B., Greeley, R., Chuang, F. C., Klemaszewski, J., Clark, R. N., Dalton, J. B., Hibbitts, C. A., Schenk, P. M., Spencer, J. R., and Wagner, R. (2004). *Callisto*, volume 1, pages 397–426.

Mueller, S. and McKinnon, W. B. (1988). Three-layered models of Ganymede and Callisto: Compositions, structures, and aspects of evolution. *Icarus*, 76(3):437–464.

Nimmo, F. and Pappalardo, R. T. (2004). Furrow flexure and ancient heat flux on Ganymede. *Geophysical Research Letters*, 31(19):L19701.

Nunes, D. C. and Phillips, R. J. (2006). Radar subsurface mapping of the polar layered deposits on Mars. *Journal of Geophysical Research (Planets)*, 111(E6):E06S21.

Ogihara, M. and Ida, S. (2012). N-body Simulations of Satellite Formation around Giant Planets: Origin of Orbital Configuration of the Galilean Moons. *Astrophysical Journal*, 753(1):60.

Ostro, S. J. and Shoemaker, E. M. (1990). The extraordinary radar echoes from Europa, Ganymede, and Callisto: A geological perspective. *Icarus*, 85(2):335–345.

Pappalardo, R. T., Belton, M. J. S., Breneman, H. H., Carr, M. H., Chapman, C. R., Collins, G. C., Denk, T., Fagents, S., Geissler, P. E., Giese, B., Greeley, R., Greenberg, R., Head, J. W., Helfenstein, P., Hoppa, G., Kadel, S. D., Klaasen, K. P., Klemaszewski, J. E., Magee, K., McEwen, A. S., Moore, J. M., Moore, W. B., Neukum, G., Phillips, C. B., Prockter, L. M., Schubert, G., Senske, D. A., Sullivan, R. J., Tufts, B. R., Turtle, E. P., Wagner, R., and Williams, K. K. (1999). Does Europa have a subsurface ocean? Evaluation of the geological evidence. *Journal of Geophysical Research*, 104(E10):24015–24056.

Pappalardo, R. T., Collins, G. C., Head, James W., I., Helfenstein, P., McCord, T. B., Moore, J. M., Prockter, L. M., Schenk, P. M., and Spencer, J. R. (2004). *Geology of Ganymede*, volume 1, pages 363–396.

Peale, S. J. and Lee, M. H. (2002). A Primordial Origin of the Laplace Relation Among the Galilean Satellites. *Science*, 298(5593):593–597.

Pettinelli, E., Cosciotti, B., Di Paolo, F., Lauro, S., Mattei, E., Orosei, R., and Vannaroni, G. (2015). Dielectric properties of jovian satellite ice analogs for subsurface radar exploration: A review: Jovian icy moons dielectric properties. *Reviews of Geophysics*, 53:n/a–n/a.

Schenk, P. M. and McKinnon, W. B. (1991). Dark-ray and dark-floor craters on Ganymede, and the provenance of large impactors in the Jovian system. *Icarus*, 89(2):318–346.

Schubert, G., Stevenson, D. J., and Ellsworth, K. (1981). Internal structures of the Galilean satellites. *Icarus*, 47(1):46–59.

Showman, A. P. and Malhotra, R. (1999). The Galilean satellites. *Science*, 296(5437):77–84.

Sohl, F., Spohn, T., Breuer, D., and Nagel, K. (2002). Implications from Galileo Observations on the Interior Structure and Chemistry of the Galilean Satellites. *Icarus*, 157(1):104–119.

Sotin, C., Reynard, B., Guyot, F., and Neri, A. (2020). Interior Structure Models Suggest a Cometary Origin for the Large Icy Moons. In *Lunar and Planetary Science Conference*, Lunar and Planetary Science Conference, page 1598.

Stephan, K., Hoffmann, H., Hibbitts, C. A., Wagner, R., and Jaumann, R. (2017). Ice particle size variations and candidate non-ice materials on Ganymede and Callisto. In *European Planetary Science Congress*, pages EPSC2017–350.

Vance, S., Bouffard, M., Choukroun, M., and Sotin, C. (2014). Ganymede's internal structure including thermodynamics of magnesium sulfate oceans in contact with ice. *Planetary and Space Science*, 96:62–70.

Yoder, C. F. and Peale, S. J. (1981). The tides of Io. *Icarus*, 47(1):1–35.